solids

MDPI

Article

About the Rare-Earth Metal(III) Bromide Oxoarsenates(III) $RE_5Br_3[AsO_3]_4$ with *A*- (*RE* = La and Ce) or *B*-Type Structure (*RE* = Pr, Nd, Sm–Tb) and $RE_3Br_2[AsO_3][As_2O_5]$ (*RE* = Y, Dy–Yb)

Ralf J. C. Locke [1], Florian Ledderboge [1,2], Felix C. Goerigk [1,3], Frank C. Zimmer [1] and Thomas Schleid [1,*]

[1] Institute for Inorganic Chemistry, University of Stuttgart, D-70569 Stuttgart, Germany
[2] Bundesamt für Infrastruktur, Umweltschutz und Dienstleistungen der Bundeswehr, D-53123 Bonn, Germany
[3] Leuchtstoffwerk Breitungen GmbH, D-98597 Breitungen, Germany
* Correspondence: thomas.schleid@iac.uni-stuttgart.de

Abstract: The monoclinic rare-earth metal(III) bromide oxoarsenates(III) $RE_5Br_3[AsO_3]_4$ of the *A*-type (RE = La and Ce) crystallize in the space group $C2/c$ with the lattice parameters a = 1834.67(9) pm, b = 553.41(3) pm, c = 1732.16(9) pm and β = 107.380(3)° for $La_5Br_3[AsO_3]_4$ and a = 1827.82(9) pm, b = 550.67(3) pm, c = 1714.23(9) pm and β = 107.372(3)° for $Ce_5Br_3[AsO_3]_4$ with Z = 4, while, for the *B*-type (*RE* = Pr, Nd and Sm–Tb), they prefer the space group $P2/c$ with lattice parameters from a = 881.23(5) pm, b = 547.32(3) pm, c = 1701.14(9) pm and β = 90.231(3)° for $Pr_5Br_3[AsO_3]_4$ to a = 875.71(5) pm, b = 535.90(3) pm, c = 1643.04(9) pm and β = 90.052(3)° for $Tb_5Br_3[AsO_3]_4$ with Z = 2. The closely related rare-earth metal(III) bromide oxoarsenates(III) $RE_3Br_2[AsO_3][As_2O_5]$ crystallize in the triclinic space group $P\bar{1}$ with lattice parameters from a = 539.15(4) pm, b = 870.68(6) pm, c = 1092.34(8), α = 90.661(2)°, β = 94. 792(2)° and γ = 90.223(2)° for $Dy_3Br_2[AsO_3][As_2O_5]$ to a = 533.56(4) pm, b = 869.61(6) pm, c = 1076.70(8), α = 90.698(2)°, β = 94.785(2)° and γ = 90.053(2)° for $Yb_3Br_2[AsO_3][As_2O_5]$ with Z = 2. All three structures have the same building units with $[REO_8]^{13-}$ and $[REO_4Br_4]^{9-}$ polyhedra as well as isolated ψ^1-tetrahedral $[AsO_3]^{3-}$ anions in common, with the exception that, in the latter two, ψ^1-$[AsO_3]^{3-}$ tetrahedra linked by a corner form a pyroanionic $[As_2O_5]^{4-}$ entity. *A*- and *B*-type differ in the stacking sequence of their $^2_\infty\{[(RE3)O^{t}_{4/1}(Br1)^{v}_{1/2}(Br2)^{e}_{3/3}]^{6.5-}\}$ layers. While the former have an ABC sequence, the latter exhibit an AAA variant. In the triclinic structures, the $(RE3)^{3+}$ sites are thinned out, while the As^{3+} sites are simultaneously enriched, resulting in the mentioned condensed units.

Keywords: rare-earth metals; bromides; oxoarsenates(III); crystal-structure comparison; single crystals

Academic Editor: Timothy J. Prior

Received: 10 December 2024
Revised: 30 December 2024
Accepted: 7 January 2025
Published: 15 January 2025

Citation: Locke, R.J.C.; Ledderboge, F.; Goerigk, F.C.; Zimmer, F.C.; Schleid, T. About the Rare-Earth Metal(III) Bromide Oxoarsenates(III) $RE_5Br_3[AsO_3]_4$ with *A*- (*RE* = La and Ce) or *B*-Type Structure (*RE* = Pr, Nd, Sm–Tb) and $RE_3Br_2[AsO_3][As_2O_5]$ (*RE* = Y, Dy–Yb). *Solids* **2025**, *6*, 4. https://doi.org/10.3390/solids6010004

1. Introduction

The rare-earth metal(III) bromide oxopnictogenates(III) have an impressive number of different structures to date, and the best-studied are the bismutates and antimonates. Only a single composition is realized with bismuth, where the tetragonal $REBrBi_2O_4$ representatives [1] with *RE* = Y, Pr, Nd and Sm–Lu crystallize in the space group $P4/mmm$. They contain $[REO_8]^{13-}$ and corner-linked ψ^1-pyramidal $[BiO_4]^{5-}$ units to form a checkerboard pattern. The bromide anions are isolated from these layers and only linked to them via secondary contacts. A very similar picture emerges for the antimonates, where there is an isostructural example with $LaBrSb_2O_4$ [2] and the cation-mixed $Sm_{1.5}BrSb_{1.5}O_4$ [3] examples. The same composition $REBrSb_2O_4$ is also known with two more different structure

types. The rare-earth metal environment does not differ apart from a slight distortion. Here, the trivalent antimony surrounds itself with three oxygen atoms to form a ψ^1-tetrahedron $[SbO_3]^{3-}$, which is linked to others via corners either to form chains $^1_\infty\{[SbO^{v}_{2/1}O^{t}_{1/1}]^-\}$ (v = vertex and t = terminal) for the monoclinic representatives crystallizing in the space group $P2_1/c$ (*RE* = Y, Nd and Eu–Dy) [4–7] or isolated rings $^0_\infty\{[(SbO^{v}_{2/1}O^{t}_{1/1})_4]^{4-}\}$ for the tetragonal representatives (*RE* = Er and Tm) [5,8] adopting the space group $P42_12$. Furthermore, there is the orthorhombically crystallizing (space group: *Pnma*) $La_2Br_4Sb_{12}O_{19}$ [9], which features edge-linked, capped square prisms $[LaO_9]^{15-}$, located within double-halfpipes of linked ψ^1-pyramidal $[SbO_4]^{5-}$ and ψ^1-tetrahedral $[SbO_3]^{3-}$ groups. For charge neutrality, only bromide anions that are only bound via secondary contacts again are located between these $^1_\infty\{[Sb_{12}O_{19}]^{2-}\}$ strands. In the case of arsenates, only two different examples are known to date, firstly tetragonal $La_3OBr[AsO_3]_2$ (space group: $P4_2/mnm$) [10], which displays trigonal prisms of oxygen around lanthanum that are doubly capped by bromide anions $[LaO_6Br_2]^{11-}$ and an additional trigonal prism $[LaO_8Br]^{12-}$, which is tricapped by two oxygen atoms and a bromide anion. The ψ^1-tetrahedral $[AsO_3]^{3-}$ anions are isolated here, but arranged in such a way that lone-pair channels form. Furthermore, $Tm_3Br_2[AsO_3][As_2O_5]$ (space group: $P\bar{1}$) [11] is another individual case whose significantly extended series is presented for the first time in this publication, supplemented and compared with the previously completely unknown series of $RE_5Br_3[AsO_3]_4$ representatives with *RE* = La–Nd and Sm–Tb, moreover.

2. Materials and Methods

The new rare-earth metal(III) bromide oxoarsenates(III) with the composition $RE_5Br_3[AsO_3]_4$ were produced for *RE* = La–Nd and Sm–Tb via a metallothermic reaction of rare-earth metal (*RE*: ChemPur, Karlsruhe, Germany, 99.9%) with rare-earth metal tribromide ($REBr_3$: ChemPur, 99.99%) and arsenic sesquioxide (As_2O_3: Aldrich, Darmstadt, Germany, 99.99%) using cesium bromide (CsBr: Merck, Darmstadt, Germany, 99.9%) as flux according to Equation (1) at temperatures of 825 °C, as no single crystals of sufficient size for single crystal X-ray analysis were obtained at lower temperatures:

$$4\ RE + REBr_3 + 4\ As_2O_3 \rightarrow RE_5Br_3[AsO_3]_4 + 4\ As\ (RE = La–Nd, Sm–Tb) \quad (1)$$

The also new rare-earth metal(III) bromide oxoarsenates(III) with the composition $RE_3Br_2[AsO_3][As_2O_5]$ with *RE* = Y and Dy–Yb were obtained from the rare-earth metal sesquioxides (RE_2O_3: ChemPur, 99.9%) with rare-earth metal bromide ($REBr_3$: ChemPur, 99.99%) and arsenic sesquioxide (As_2O_3: Aldrich, 99.99%) again with cesium bromide (CsBr: Merck, 99.9%) as a fluxing agent according to Equation (2) at temperatures of 780 °C, as no single crystals of sufficient size for single crystal X-ray analysis were obtained at lower temperatures:

$$7\ RE_2O_3 + 4\ REBr_3 + 9\ As_2O_3 \rightarrow 6\ RE_3Br_2[AsO_3][As_2O_5]\ (RE = Y \text{ and } Dy–Yb) \quad (2)$$

After removal of the cesium–bromide flux by rinsing off with water and subsequent drying of the crude batches, suitable crystals for single-crystal X-ray structure analysis were detected and selected in all cases. The always platelet-shaped crystals were transferred into glass capillaries (Hilgenberg, Malsfeld, Germany; outer diameter: 0.1 mm, wall thickness: 0.01 mm) and fixed there with grease. For all $RE_5Br_3[AsO_3]_4$ representatives (*RE* = La–Nd and Sm–Tb), the measurements were carried out on a STADI-VARI single-crystal X-ray diffractometer (Stoe & Cie, Darmstadt, Germany), while, for the $RE_3Br_2[AsO_3][As_2O_5]$ representatives (*RE* = Y and Dy–Yb), they took place with a κ-CCD single-crystal X-ray diffrac-

tometer (Bruker-Nonius, Karlsruhe, Germany), using Mo-K_α radiation (λ = 71.07 pm) in all cases.

The monoclinic structures for *A*-type $RE_5Br_3[AsO_3]_4$ (*RE* = La and Ce) could be solved and refined in the space group $C2/c$ and for *B*-type $RE_5Br_3[AsO_3]_4$ (*RE* = Pr, Nd and Sm–Tb) in the space group $P2/c$ by direct methods using the SHELX-97 program package [12–14]. The triclinic structures of the $RE_3Br_2[AsO_3][As_2O_5]$ representatives with *RE* = Y and Dy–Yb were solved and refined with the same methods in the space group $P\bar{1}$.

3. Results and Discussion

3.1. Crystal Structure of A-Type $RE_5Br_3[AsO_3]_4$ (RE = La and Ce)

The rare-earth metal(III) bromide oxoarsenates(III) $RE_5Br_3[AsO_3]_4$ (*RE* = La and Ce) of the *A*-type crystallize isotypically to their chloride analogs $RE_5Cl_3[AsO_3]_4$ with *RE* = La–Pr [15,16] in the monoclinic space group $C2/c$ (no. 15) with lattice parameters of a = 1834.67(9) pm, b = 553.41(3) pm, c = 1732.16(9) pm and β = 107.380(3)° for $La_5Br_3[AsO_3]_4$ and a = 1827.82(9) pm, b = 550.67(3) pm, c = 1714.23(9) pm and β = 107.372(3)° for $Ce_5Br_3[AsO_3]_4$ with Z = 4.

The crystal structure contains three crystallographically different RE^{3+} cations. $(RE1)^{3+}$ is surrounded by eight oxygen atoms (d(La1–O) = 245–260 pm and d(Ce1–O) = 241–255 pm) in the shape of a slightly distorted square antiprism (Figure 1, *top left*), and, similarly, the $(RE2)^{3+}$ cation has eight O^{2-} anions arranged as a heavily distorted square hemiprism (d(La2–O) = 234–268 pm and d(Ce2–O) = 230–261 pm; Figure 1, *top mid*) as a first coordination sphere. The $(RE3)^{3+}$ cation, on the other hand, is coordinated by four oxygen atoms (d(La3–O) = 237–258 pm and d(Ce3–O) = 233–259 pm) and four Br^- anions (d(La3–Br) = 318–327 pm and d(Ce3–Br) = 316–325 pm) in the form of a square antiprism (Figure 1, *top right*).

All six crystallographically independent oxygen atoms belong to two types of isolated, ψ^1-tetrahedral oxoarsenate(III) anions $[AsO_3]^{3-}$ (Figure 2), which are formed from three oxygen atoms and a non-bonding electron pair around each As^{3+} center. The $(As1)^{3+}$ cation is coordinated by three oxygen atoms (O1, O2 and O3) with distances of d(As1–O) = 173–181 pm for $La_5Br_3[AsO_3]_4$ and d(As1–O) = 175–180 pm for $Ce_5Br_3[AsO_3]_4$. For the $(As2)^{3+}$ cation, the three oxygen ligands (O4, O5 and O6) occur with slightly longer distances (d(As2–O) = 174–182 pm for $La_5Br_3[AsO_3]_4$ and d(As1–O) = 177–184 pm for $Ce_5Br_3[AsO_3]_4$) than in the first case. Each oxygen atom of the two different discrete $[AsO_3]^{3-}$ anions is coordinated by six RE^{3+} cations each, both via corners (4×) and via edges (2×).

In the crystal structure, the $[(RE1)O_8]^{13-}$ and $[(RE2)O_8]^{13-}$ polyhedra are connected to each other by oxygen-edge bonding to form fluorite-related layers $^2_\infty\{[(RE1/2)O^e_{8/2}]^{5-}\}$ parallel to the (100) plane (Figure 1). In turn, the polyhedral $[(RE3)O_4Br_4]^{9-}$ around $(RE3)^{3+}$ attach to these layers. Thus, bilayers result from the fused rare-earth metal-oxygen polyhedra, which, together with the isolated oxoarsenate(III) anions $[AsO_3]^{3-}$, display the composition $^2_\infty\{RE_5[AsO_3]_4\}^{3+}$ and are stacked along the *a*-axis (Figure 3). Between these cationic bilayers reside the bromide anions $(Br1)^-$ and $(Br2)^-$. The two distinct Br^- anions are only surrounded by $(RE3)^{3+}$ cations. The first anion $(Br1)^-$ is linearly coordinated by two equidistant $(RE3)^{3+}$ cations (d(Br1–La3) = 318 pm and d(Br1–Ce3) = 316 pm) at an angle of 180°, whereas the $(Br2)^-$ anion shows a surrounding of three $(RE3)^{3+}$ cations (d(Br2–La3) = 319–327 pm and d(Br2–Ce3) = 317–325 pm) in the shape of a pyramid. The $[(RE3)O_4Br_4]^{9-}$ polyhedra, which contain the two crystallographically different Br^- anions, are linked via bromide corners and edges to form corrugated intermediate layers (Figure 1), in which all oxygen atoms of the $[(RE3)O_4Br_4]^{9-}$ polyhedra work as components of the

isolated $[AsO_3]^{3-}$ units in such a way that the lone pairs on the As^{3+} cations point into the direction of the interlayers (Figure 3).

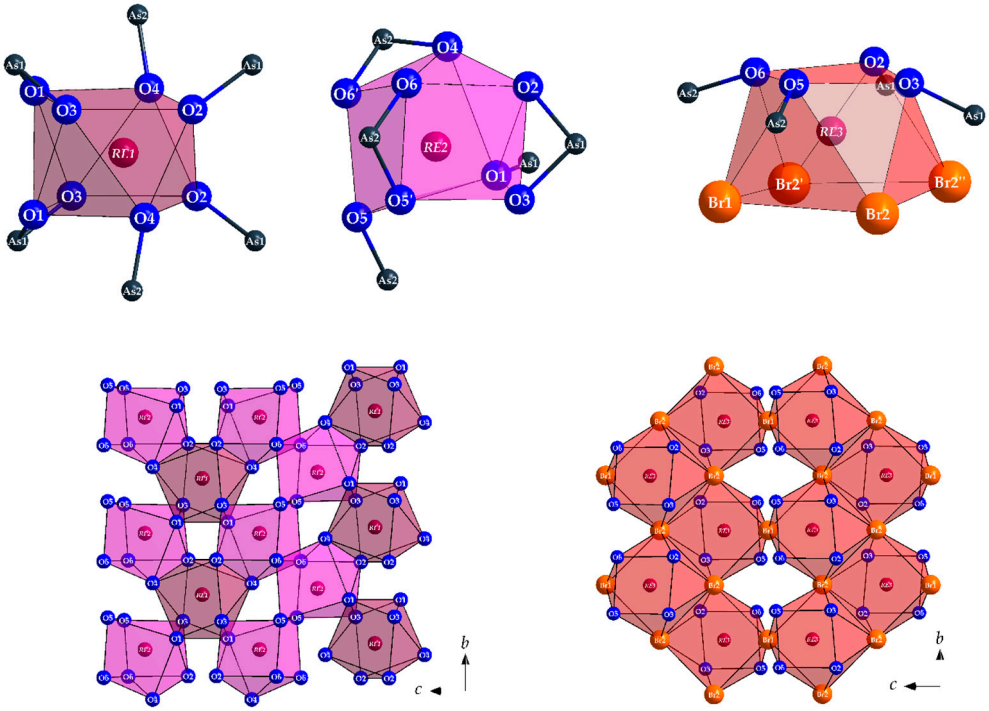

Figure 1. Slightly distorted square antiprism $[(RE1)O_8]^{13-}$ (*top left*), heavily distorted hemiprism $[(RE2)O_8]^{13-}$ (*top mid*) and square antiprism $[(RE3)O_4Br_4]^{9-}$ (*top right*) with the environment of As^{3+} cations in the crystal structure of the $RE_5Br_3[AsO_3]_4$ representatives of the *A*-type (*RE* = La and Ce) and their linkage to $^{2}_{\infty}\{[(RE1/2)O^{e}_{8/2}]^{5-}\}$ layers (*bottom left*) and $^{2}_{\infty}\{[(RE3)O^{t}_{4/1}(Br1)^{v}_{1/2}(Br2)^{e}_{3/3}]^{6.5-}\}$ layers with linearly coordinated $(Br1)^{-}$ and trigonally non-planar coordinated $(Br2)^{-}$ anions (*bottom right*).

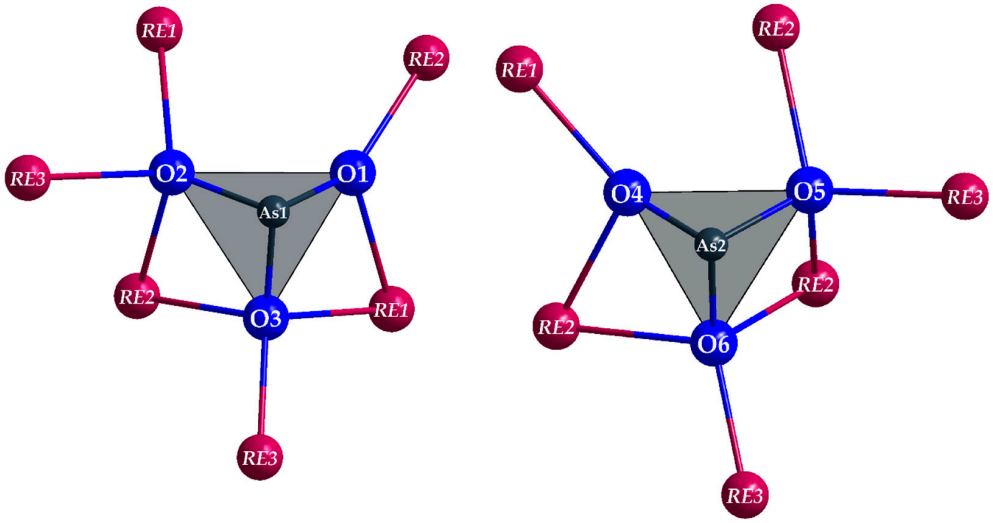

Figure 2. Irregular environment of RE^{3+} cations around the discrete ψ^1-tetrahedral $[(As1)O_3]^{3-}$ and $[(As2)O_3]^{3-}$ anions in the crystal structure of the $RE_5Br_3[AsO_3]_4$ representatives of the *A*-type (*RE* = La and Ce).

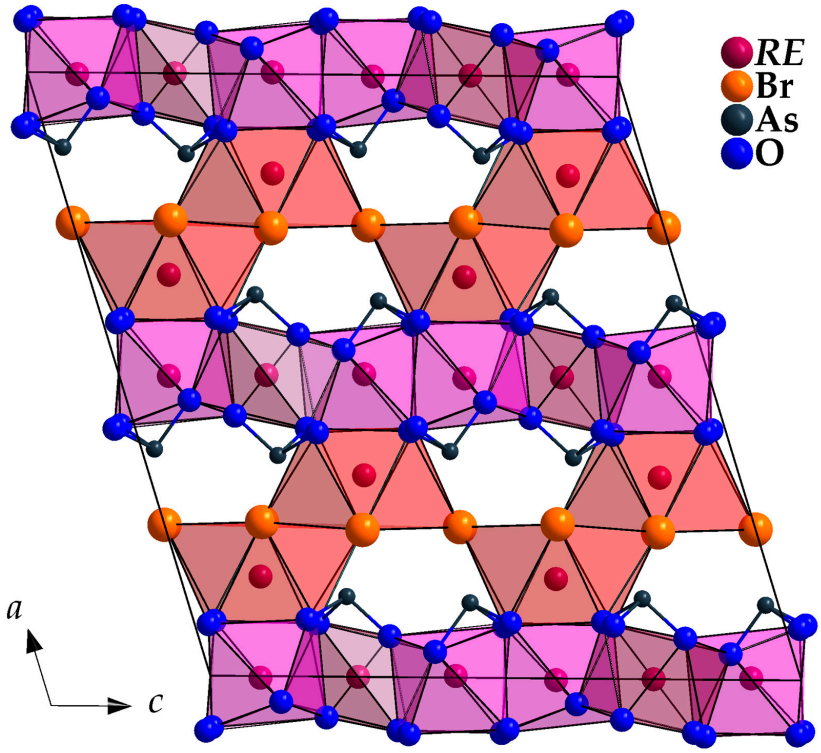

Figure 3. Extended unit cell of the $RE_5Br_3[AsO_3]_4$ representatives with the *A*-type structure (*RE* = La and Ce).

Table 1 contains the crystallographic data for *A*-type $La_5Br_3[AsO_3]_4$ and $Ce_5Br_3[AsO_3]_4$ with their determination, Table 2 the fractional atomic positions along with the coefficients of equivalent isotropic displacement parameters and Table 3 selected interatomic distances.

Table 1. Crystallographic data of *A*-type $RE_5Br_3[AsO_3]_4$ (*RE* = La and Ce).

$RE_5Br_3[AsO_3]_4$		La	Ce
Crystal system		monoclinic	
Space group		$C2/c$ (no. 15)	
Lattice parameters,	a/pm	1834.67(9)	1827.82(9)
	b/pm	553.41(3)	550.67(3)
	c/pm	1732.16(9)	1714.23(9)
	β/°	107.380(3)	107.372(3)
Formula units, Z		4	
Calculated density, D_x/g·cm^{-3}		5.643	5.776
Molar volume, V_m/cm^3·mol^{-1}		252.69(9)	247.92(9)
Diffractometer		STADI-VARI (Stoe & Cie)	
Wavelength		Mo-K_α (λ = 71.07 pm)	
Electron sum, $F(000)$/e$^-$		2472	2492
Measurement limit, θ_{max}/°		33.00	32.85
Measurement range, $\pm h/\pm k/\pm l_{min/max}$		27/8/26	27/8/25
Observed reflections		20793	18462
Unique reflections		3010	2917
Absorption coefficient, μ/mm^{-1}		27.47	28.85
R_{int}/R_σ		0.096/0.053	0.045/0.039
R_1/R_1 with $\|F_o\| \geq 4\sigma(F_o)$		0.084/0.056	0.066/0.036
wR_2/Goof		0.089/0.873	0.084/0.990
Residual electron density, ρ/e$^-$·10^{-6}·pm^{-3}		−2.54/2.73	−2.17/2.26
CSD number		2263604	2263605

Table 2. Fractional atomic coordinates and coefficients of the equivalent isotropic displacement parameters for the *A*-type $RE_5Br_3[AsO_3]_4$ representatives with *RE* = La and Ce.

Atom	*Wyckoff* Site	*x*/*a*	*y*/*b*	*z*/*c*	U_{eq}/pm^2
		$La_5Br_3[AsO_3]_4$			
La1	4*e*	0	0.21052(19)	$^1/_4$	55(3)
La2	8*f*	0.49637(4)	0.23925(16)	0.08362(4)	44(2)
La3	8*f*	0.16655(5)	0.24725(16)	0.13643(4)	47(2)
Br1	4*c*	$^1/_4$	$^1/_4$	0	154(4)
Br2	8*f*	0.24296(7)	0.2473(3)	0.33316(7)	92(3)
As1	8*f*	0.36697(7)	0.2569(3)	0.22902(7)	43(3)
As2	8*f*	0.12415(7)	0.2579(3)	0.47883(7)	59(3)
O1	8*f*	0.4310(6)	0.3300(14)	0.1769(6)	155(24)
O2	8*f*	0.4083(7)	0.0106(14)	0.2901(7)	108(30)
O3	8*f*	0.4056(7)	0.4829(14)	0.3060(7)	88(27)
O4	8*f*	0.0444(6)	0.3002(14)	0.3949(6)	108(22)
O5	8*f*	0.0867(7)	0.0123(14)	0.5257(7)	99(31)
O6	8*f*	0.0919(7)	0.4932(14)	0.5341(7)	98(30)
		$Ce_5Br_3[AsO_3]_4$			
Ce1	4*e*	0	0.21009(9)	$^1/_4$	94(1)
Ce2	8*f*	0.49725(2)	0.23741(7)	0.08394(2)	93(1)
Ce3	8*f*	0.16519(2)	0.24647(7)	0.13604(2)	99(1)
Br1	4*c*	$^1/_4$	$^1/_4$	0	194(2)
Br2	8*f*	0.24408(4)	0.24738(11)	0.33314(4)	133(1)
As1	8*f*	0.36673(4)	0.25801(11)	0.22788(4)	89(1)
As2	8*f*	0.12440(4)	0.25794(11)	0.47806(4)	99(1)
O1	8*f*	0.4322(3)	0.3334(8)	0.1754(3)	144(10)
O2	8*f*	0.4117(3)	0.0093(7)	0.2908(3)	122(10)
O3	8*f*	0.4055(3)	0.4811(7)	0.3064(3)	102(10)
O4	8*f*	0.0426(3)	0.3086(8)	0.3934(3)	204(11)
O5	8*f*	0.0855(3)	0.0115(7)	0.5236(3)	109(10)
O6	8*f*	0.0913(3)	0.4954(7)	0.5354(3)	103(10)

Table 3. Selected interatomic distances (d/pm) for the *A*-type $RE_5Br_3[AsO_3]_4$ representatives with *RE* = La and Ce.

RE		**La**	**Ce**
$[(RE1)O_8]^{13-}$ polyhedron			
*RE*1–O4	2×	244.7(8)	240.9(5)
*RE*1–O3	2×	255.5(12)	255.0(5)
*RE*1–O1	2×	258.6(8)	255.5(5)
*RE*1–O2	2×	260.2(10)	254.7(5)
$[(RE2)O_8]^{13-}$ polyhedron			
*RE*2–O1	1×	233.7(10)	229.5(5)
*RE*2–O6	1×	252.1(10)	247.9(5)
*RE*2–O5	1×	254.3(10)	251.0(5)
*RE*2–O5′	1×	257.6(12)	256.4(5)
*RE*2–O3	1×	258.0(11)	255.0(5)
*RE*2–O6′	1×	258.1(12)	257.0(5)
*RE*2–O4	1×	260.2(8)	253.5(5)
*RE*2–O2	1×	267.6(13)	261.2(5)
$[(RE3)O_4Br_4]^{9-}$ polyhedron			
*RE*3–O6	1×	237.2(12)	233.0(4)
*RE*3–O3	1×	238.3(10)	235.4(4)
*RE*3–O5	1×	249.2(11)	248.5(4)
*RE*3–O2	1×	258.3(10)	258.7(5)
*RE*3–Br1	1×	317.65(7)	316.24(4)
*RE*3–Br2	1×	318.82(14)	317.17(7)
*RE*3–Br2′	1×	318.91(14)	318.04(7)
*RE*3–Br2″	1×	327.47(14)	325.35(7)
$[(As1)O_3]^{3-}$ anion			
As1–O1	1×	173.0(10)	174.8(5)
As1–O2	1×	175.3(10)	178.4(4)
As1–O3	1×	181.1(10)	180.3(4)
$[(As2)O_3]^{3-}$ anion			
As2–O4	1×	174.3(9)	176.7(5)
As2–O5	1×	181.7(10)	181.4(4)
As2–O6	1×	182.0(10)	184.3(4)

3.2. Crystal Structure of B-Type $RE_5Br_3[AsO_3]_4$ (RE = Pr, Nd and Sm–Tb)

The rare-earth metal(III) bromide oxoarsenates(III) $RE_5Br_3[AsO_3]_4$ (*RE* = Pr, Nd and Sm–Tb) of the *B*-type crystallize isotypically to $La_5Cl_3[SbO_3]_4$ [9] in the monoclinic space group $P2/c$ (no. 13) with lattice parameters from a = 881.23(5) pm, b = 547.32(3) pm, c = 1701.14(9) pm and β = 90.231(3)° for $Pr_5Br_3[AsO_3]_4$ to a = 875.71(5) pm, b = 535.90(3) pm, c = 1643.04(9) pm and β = 90.052(3)° for $Tb_5Br_3[AsO_3]_4$ with Z = 2 nicely reflecting the consequences of the lanthanoid contraction. Three crystallographically different rare-earth metal(III) cations are present in the crystal structure, and all of them are surrounded by eight anions. In the case of the $(RE1)^{3+}$ and $(RE2)^{3+}$ cations, one finds exclusively O^{2-} anions, which form distorted square antiprisms $[(RE1)O_8]^{13-}$ (d(Pr1–O) = 238–254 pm to d(Tb1–O) = 227–246 pm) or distorted cubes $[(RE2)O_8]^{13-}$ (d(Pr2–O) = 227–259 pm to d(Tb2–O) = 219–253 pm) (Figure 4, *top left and mid*). Six As^{3+} cations (2× edge and 4× corner) graft at the $[(RE1)O_8]^{13-}$ polyhedron, whereas there are only five of them (2× edge and 3× corner) in the case of the $[(RE2)O_8]^{13-}$ polyhedron. These two types of polyhedra are linked via four of their edges to form layers $^2_\infty\{[(RE1/2)O^e_{8/2}]^{5-}\}$ within the (100) plane. It can be seen that each $[(RE1)O_8]^{13-}$ polyhedron is linked to four $[(RE2)O_8]^{13-}$ polyhedra, whilst each $[(RE2)O_8]^{13-}$ polyhedron joins with two $[(RE1)O_8]^{13-}$ and two $[(RE2)O_8]^{13-}$ polyhedra (Figure 4, *below left*). The two crystallographically different Br^-

anions occur in the crystal structure, resulting in a different bonding arrangement around the $(RE3)^{3+}$ cations. While the $(Br1)^{-}$ anions are linearly surrounded by two $(RE3)^{3+}$ cations $[(Br1)RE_2]^{5+}$, the $(Br2)^{-}$ anions show a trigonal non-planar environment $[(Br2)RE_3]^{8+}$. However, the square antiprism $[(RE3)O_4Br_4]^{9-}$ formed by four O^{2-} and four Br^{-} anions around each $(RE3)^{3+}$ cation is only slightly distorted (Figure 4, *top right*). The distances of contacts to the O^{2-} anions show a greater variance with *d*(Pr3–O) = 228–253 pm to *d*(Tb3–O) = 220–245 pm and *d*(Pr3–Br) = 316–320 pm to *d*(Tb3–Br) = 313–318 pm. Once again, the bromide anions are only connected to the rest of the structure via these $(RE3)^{3+}$ cations. The $[(RE3)O_4Br_4]^{9-}$ antiprisms share common edges of $(Br2)^{-}$ anions to form bands that run along [010] and are finally corner-linked via $(Br1)^{-}$ anions to create two-dimensional bilayers of composition ${}^{2}_{\infty}\{[(RE3)O^{t}_{4/1}(Br1)^{v}_{1/2}(Br2)^{e}_{3/3}]^{6.5-}\}$, also spreading out parallel to the (100) plane (Figure 4, *bottom right*).

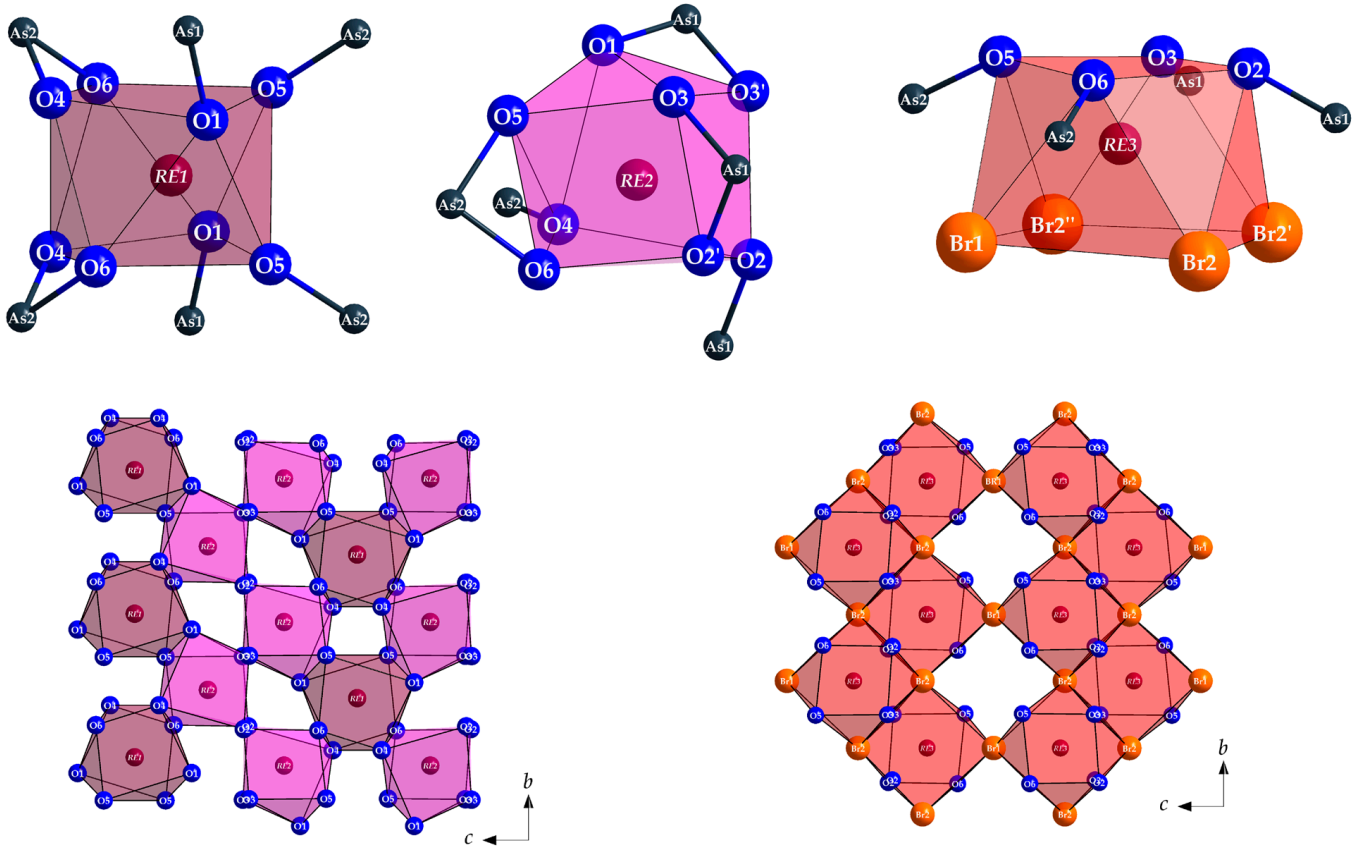

Figure 4. Distorted square antiprism $[(RE1)O_8]^{13-}$ (*top left*), highly distorted cube $[(RE2)O_8]^{13-}$ (*top mid*) and square antiprism $[(RE3)O_4Br_4]^{9-}$ (*top right*) with their environment of As^{3+} cations in the crystal structure of the *B*-type $RE_5Br_3[AsO_3]_4$ representatives (*RE* = Pr, Nd and Sm–Tb) and their linkage to layers ${}^{2}_{\infty}\{[(RE1/2)O^{e}_{8/2}]^{5-}\}$ (*bottom left*) and ${}^{2}_{\infty}\{[(RE3)O^{t}_{4/1}(Br1)^{v}_{1/2}(Br2)^{e}_{3/3}]^{6.5-}\}$ with linearly coordinated $(Br1)^{-}$ and trigonally non-planar coordinated $(Br2)^{-}$ anions (*bottom right*).

As expected, both kinds of As^{3+} cations are surrounded by three O^{2-} anions to form tripodal ψ^1 tetrahedra (*d*(As–O) = 175–185 pm for $Pr_5Br_3[AsO_3]_4$ to *d*(As–O) = 176–184 pm for $Tb_5Br_3[AsO_3]_4$). In the next coordination sphere, one finds six RE^{3+} cations, which are twice edge-bridging and four times terminally bound to the oxide anions (Figure 5). A view from the oxygen atoms shows that one of the three O^{2-} ligands is only further coordinated by two RE^{3+} cations, while the remaining two have three contacts each. This is also reflected in the distances to the central As^{3+} cations, as the former are the shortest in both $[AsO_3]^{3-}$ units.

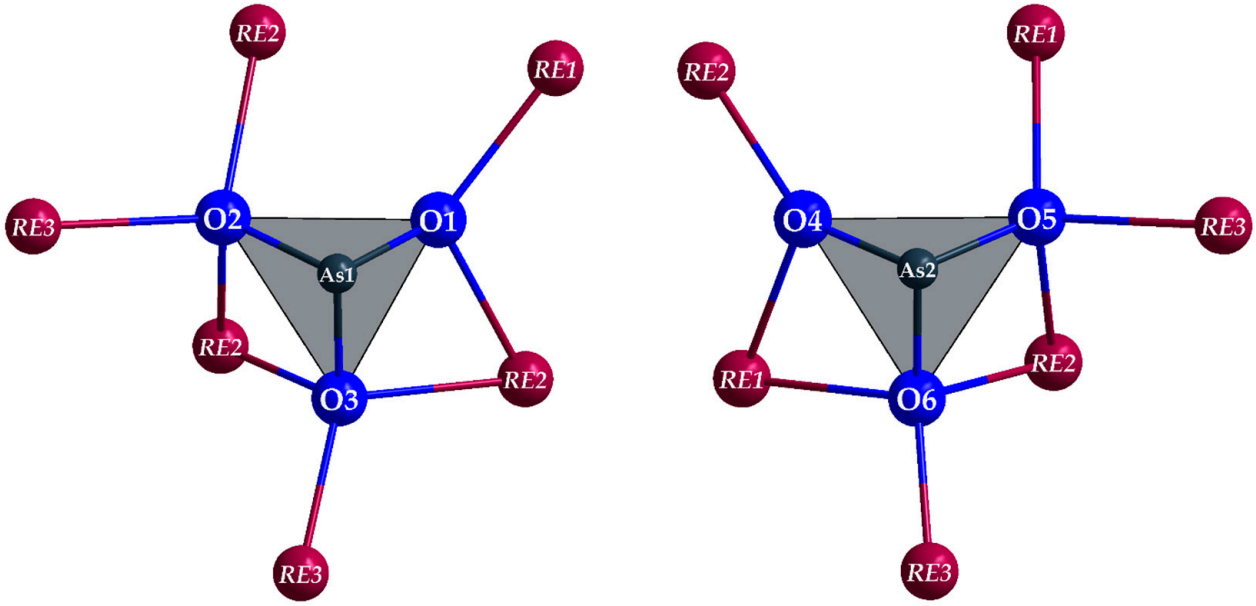

Figure 5. Irregular environment of RE^{3+} cations around the ψ^1-tetrahedral $[(As1)O_3]^{3-}$ and $[(As2)O_3]^{3-}$ anions in the crystal structure of the *B*-type $RE_5Br_3[AsO_3]_4$ representatives (*RE* = Pr, Nd and Sm–Tb).

Within the crystal structure, open channels remain between the bromide anion and rare-earth metal bilayers, into which the free electron pairs of the As^{3+} cations point (Figure 6).

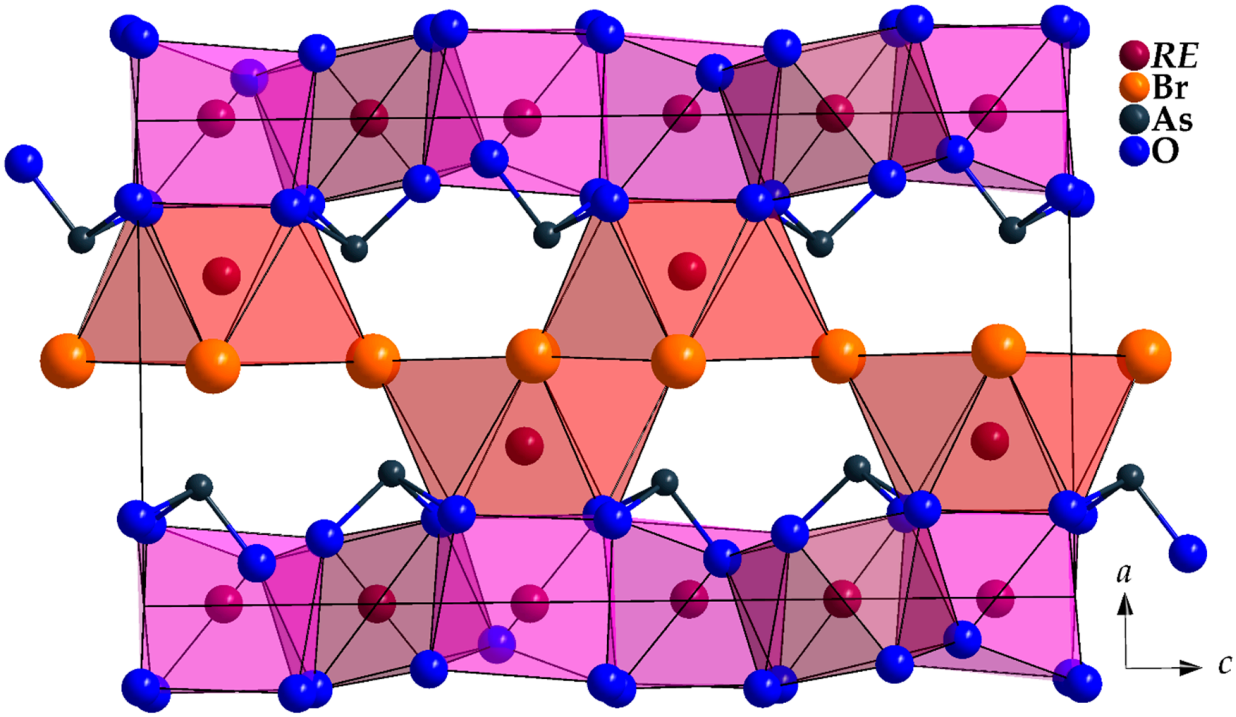

Figure 6. Extended unit cell of the *B*-type $RE_5Br_3[AsO_3]_4$ representatives (*RE* = Pr, Nd and Sm–Tb).

Table 4 contains the crystallographic data for the *B*-type $RE_5Br_3[AsO_3]_4$ series with *RE* = Pr, Nd and Sm–Tb, and Table 5 the fractional atomic positions and U_{eq} values, while Table 6 shows a compilation of selected distances.

Table 4. Crystallographic data of the *B*-type $RE_5Br_3[AsO_3]_4$ series (*RE* = Pr, Nd and Sm–Tb) and their determination.

$RE_3Br_3[AsO_3]_4$		Pr	Nd	Sm	Eu	Gd	Tb
Crystal system				monoclinic			
Space group				*P*2/*c* (no. 13)			
Lattice parameters,	*a*/pm	881.23(5)	880.34(5)	878.46(5)	877.59(5)	876.64(5)	875.71(5)
	b/pm	547.32(3)	544.53(3)	541.19(3)	539.46(3)	537.71(3)	535.90(3)
	c/pm	1701.14(9)	1689.75(9)	1669.37(9)	1660.68(9)	1651.85(9)	1643.04(9)
	β/°	90.231(3)	90.196(3)	90.134(3)	90.107(3)	90.078(3)	90.052(3)
Formula units, *Z*				2			
Calculated density, D_x/g·cm^{-3}		5.812	5.956	6.206	6.299	6.473	6.573
Molar volume, V_m/cm^3·mol^{-1}		247.06(9)	243.89(9)	238.99(9)	236.74(9)	234.46(9)	232.16(9)
Diffractometer				STADI-VARI (Stoe & Cie)			
Wavelength				Mo-K_α (λ = 71.07 pm)			
Electron sum, *F*(000)/e$^-$		1256	1266	1286	1296	1306	1316
Measurement limit, θ_{max}/°		32.7	32.9	32.9	33.0	32.9	32.9
Measurement range, $\pm h/\pm k/\pm l_{min/max}$		12/8/25	13/8/25	13/8/25	13/8/24	12/8/24	13/8/24
Observed reflections		15554	18023	15892	17671	15396	17361
Unique reflections		2839	2877	2785	2777	2711	2754
Absorption coefficient, μ/mm^{-1}		29.93	31.30	34.09	35.68	37.19	38.98
R_{int}/R_σ		0.042/0.033	0.074/0.048	0.036/0.028	0.043/0.032	0.041/0.030	0.043/0.034
R_1/R_1 with $\|F_o\| \geq 4\sigma(F_o)$		0.057/0.040	0.091/0.045	0.032/0.023	0.042/0.027	0.042/0.033	0.046/0.030
wR_2/Goof		0.096/1.014	0.097/0.984	0.047/0.975	0.061/1.002	0.082/1.006	0.070/1.055
Residual electron density, ρ/e$^-$·10^{-6}·pm^{-3}		−3.82/4.07	−4.31/4.46	−1.69/1.82	−2.16/2.27	−3.21/3.09	−3.29/3.45
CSD number		2394253	2394254	2394255	2394256	2394257	2394258

Table 5. Fractional atomic coordinates and coefficients of the equivalent isotropic displacement parameters for the *B*-type $RE_5Br_3[AsO_3]_4$ representatives with *RE* = Pr, Nd and Sm–Tb.

Atom	*Wyckoff* Site	*x*/*a*	*y*/*b*	*z*/*c*	U_{eq}/pm^2
		$Pr_5Br_3[AsO_3]_4$			
Pr1	2*e*	0	0.20745(9)	$^1/_4$	49(1)
Pr2	4*g*	−0.00328(5)	0.73670(7)	0.41419(3)	48(1)
Pr3	4*g*	0.32308(5)	0.24892(7)	0.41123(3)	67(1)
Br1	2*f*	$^1/_2$	0.24872(18)	$^1/_4$	160(3)
Br2	4*g*	0.50807(11)	0.75073(12)	0.42162(5)	91(2)
As1	4*g*	0.24419(11)	0.25781(12)	0.06087(5)	67(2)
As2	4*g*	0.26856(11)	0.75732(12)	0.26825(5)	59(2)
O1	4*g*	0.0847(7)	0.3092(9)	0.1213(3)	138(12)
O2	4*g*	0.1686(7)	0.0113(9)	0.0044(3)	84(11)
O3	4*g*	0.1813(7)	0.5041(9)	0.4929(3)	71(11)
O4	4*g*	0.1367(7)	0.8356(9)	0.1956(3)	92(11)
O5	4*g*	0.1741(7)	0.5076(9)	0.3180(3)	81(11)
O6	4*g*	0.1848(7)	0.9818(9)	0.3369(3)	67(11)
		$Nd_5Br_3[AsO_3]_4$			
Nd1	2*e*	0	0.20605(13)	$^1/_4$	89(2)
Nd2	4*g*	−0.00298(7)	0.73582(11)	0.41428(4)	84(1)
Nd3	4*g*	0.32186(7)	0.24851(11)	0.41117(4)	104(1)
Br1	2*f*	$^1/_2$	0.2490(4)	$^1/_4$	195(3)
Br2	4*g*	0.50710(11)	0.7511(3)	0.42205(7)	130(2)
As1	4*g*	0.24423(12)	0.2583(2)	0.06137(7)	104(2)
As2	4*g*	0.26815(12)	0.7580(2)	0.26804(7)	100(2)
O1	4*g*	0.0843(9)	0.3147(14)	0.1232(5)	188(18)
O2	4*g*	0.1687(9)	0.0114(14)	0.0038(5)	101(16)
O3	4*g*	0.1802(9)	0.5023(14)	0.4918(5)	145(18)
O4	4*g*	0.1359(9)	0.8406(14)	0.1957(5)	160(17)
O5	4*g*	0.1747(9)	0.5078(14)	0.3170(5)	141(18)
O6	4*g*	0.1847(9)	0.9822(14)	0.3373(5)	90(16)

Table 5. *Cont.*

Atom	*Wyckoff* Site	*x*/*a*	*y*/*b*	*z*/*c*	U_{eq}/pm^2
		$Sm_5Br_3[AsO_3]_4$			
Sm1	2*e*	0	0.20307(7)	$^1/_4$	82(1)
Sm2	4*g*	−0.00144(4)	0.73417(6)	0.41437(2)	83(1)
Sm3	4*g*	0.31758(4)	0.24855(6)	0.41145(2)	89(1)
Br1	2*f*	$^1/_2$	0.24903(14)	$^1/_4$	186(2)
Br2	4*g*	0.50527(7)	0.75141(12)	0.42279(4)	130(1)
As1	4*g*	0.24327(8)	0.25875(11)	0.06269(4)	86(1)
As2	4*g*	0.26775(8)	0.75830(11)	0.26706(4)	81(1)
O1	4*g*	0.0843(6)	0.3210(7)	0.1234(2)	163(9)
O2	4*g*	0.1660(6)	0.0098(9)	0.0053(3)	110(9)
O3	4*g*	0.1779(6)	0.5016(9)	0.4923(3)	105(9)
O4	4*g*	0.1348(5)	0.8446(7)	0.1937(2)	123(9)
O5	4*g*	0.1729(7)	0.5024(8)	0.3168(3)	99(9)
O6	4*g*	0.1841(7)	0.9831(7)	0.3372(2)	94(9)
		$Eu_5Br_3[AsO_3]_4$			
Eu1	2*e*	0	0.20349(8)	$^1/_4$	56(1)
Eu2	4*g*	−0.00093(4)	0.73385(6)	0.41446(2)	57(1)
Eu3	4*g*	0.31635(4)	0.24839(6)	0.41165(2)	68(1)
Br1	2*f*	$^1/_2$	0.24905(16)	$^1/_4$	158(2)
Br2	4*g*	0.50475(8)	0.75134(13)	0.42294(4)	103(1)
As1	4*g*	0.24370(9)	0.25969(12)	0.06318(5)	65(1)
As2	4*g*	0.26775(9)	0.75885(12)	0.26672(5)	58(1)
O1	4*g*	0.0861(7)	0.3241(8)	0.1244(3)	157(12)
O2	4*g*	0.1654(6)	0.0109(9)	0.0065(3)	56(9)
O3	4*g*	0.1773(6)	0.5006(9)	0.4918(3)	60(9)
O4	4*g*	0.1355(6)	0.8458(8)	0.1934(3)	100(10)
O5	4*g*	0.1739(7)	0.5035(9)	0.3170(3)	82(11)
O6	4*g*	0.1830(7)	0.9822(8)	0.3385(3)	67(11)
		$Gd_5Br_3[AsO_3]_4$			
Gd1	2*e*	0	0.20140(9)	$^1/_4$	76(1)
Gd2	4*g*	−0.00089(4)	0.73331(6)	0.41445(2)	75(1)
Gd3	4*g*	0.31528(4)	0.24797(6)	0.41168(2)	80(1)
Br1	2*f*	$^1/_2$	0.24921(16)	$^1/_4$	172(3)
Br2	4*g*	0.50427(9)	0.75194(11)	0.42337(5)	122(2)
As1	4*g*	0.24290(9)	0.25997(11)	0.06338(5)	79(2)
As2	4*g*	0.26711(9)	0.75850(11)	0.26688(5)	75(2)
O1	4*g*	0.0850(7)	0.3268(9)	0.1250(3)	153(11)
O2	4*g*	0.1634(6)	0.0089(9)	0.0060(3)	93(10)
O3	4*g*	0.1775(7)	0.4993(9)	0.4926(3)	87(9)
O4	4*g*	0.1341(6)	0.8481(9)	0.1931(3)	102(10)
O5	4*g*	0.1724(7)	0.5024(9)	0.3172(3)	108(10)
O6	4*g*	0.1789(7)	0.9815(9)	0.3389(3)	96(10)
		$Tb_5Br_3[AsO_3]_4$			
Tb1	2*e*	0	0.20358(9)	$^1/_4$	88(1)
Tb2	4*g*	0.00008(5)	0.73453(7)	0.41434(3)	73(1)
Tb3	4*g*	0.31254(5)	0.24827(7)	0.41193(3)	68(1)
Br1	2*f*	$^1/_2$	0.2494(2)	$^1/_4$	162(3)
Br2	4*g*	0.50308(9)	0.75129(14)	0.42383(5)	109(2)
As1	4*g*	0.24279(9)	0.25921(13)	0.06434(5)	62(2)
As2	4*g*	0.26706(9)	0.75811(13)	0.26636(5)	65(2)
O1	4*g*	0.0841(8)	0.3303(12)	0.1258(4)	155(14)
O2	4*g*	0.1627(8)	0.0089(13)	0.0055(4)	90(12)
O3	4*g*	0.1751(9)	0.4989(14)	0.4937(4)	110(13)
O4	4*g*	0.1352(8)	0.8488(12)	0.1911(4)	116(12)
O5	4*g*	0.1734(9)	0.5009(13)	0.3171(4)	113(14)
O6	4*g*	0.1807(9)	0.9837(12)	0.3373(4)	75(13)

Table 6. Selected interatomic distances (d/pm) for the *B*-type $RE_5Br_3[AsO_3]_4$ representatives with *RE* = Pr, Nd and Sm–Tb.

RE		Pr	Nd	Sm	Eu	Gd	Tb
$[(RE1)O_8]^{13-}$ polyhedron							
*RE*1–O1	2×	238.1(6)	234.6(9)	233.0(4)	231.3(5)	229.8(5)	227.4(6)
*RE*1–O6	2×	251.8(6)	250.8(8)	247.8(5)	248.1(5)	245.1(5)	243.8(7)
*RE*1–O5	2×	252.5(6)	251.6(9)	248.4(5)	248.6(5)	247.6(5)	246.1(8)
*RE*1–O4	2×	254.2(6)	249.8(8)	246.1(4)	245.5(5)	242.4(5)	244.0(6)
$[(RE2)O_8]^{13-}$ polyhedron							
*RE*2–O4	1×	226.8(6)	226.6(8)	223.0(4)	222.8(5)	221.2(5)	218.5(6)
*RE*2–O3	1×	245.8(6)	243.3(8)	239.8(6)	238.2(6)	238.5(6)	237.4(7)
*RE*2–O6	1×	250.9(6)	249.7(8)	247.8(5)	245.0(6)	241.5(5)	242.7(7)
*RE*2–O2	1×	251.3(6)	251.2(8)	247.4(6)	245.9(6)	244.1(5)	243.5(8)
*RE*2–O1	1×	252.0(5)	248.3(8)	243.4(4)	242.0(5)	239.7(5)	238.1(6)
*RE*2–O2′	1×	255.6(6)	254.0(8)	252.6(6)	252.0(6)	250.5(5)	248.2(7)
*RE*2–O3′	1×	259.1(6)	257.9(9)	254.4(6)	253.6(6)	251.5(5)	249.1(8)
*RE*2–O5	1×	259.1(6)	259.0(9)	256.6(5)	255.4(6)	253.7(5)	253.6(7)
$[(RE3)O_4Br_4]^{9-}$ polyhedron							
*RE*3–O6	1×	228.2(5)	226.0(8)	222.9(5)	221.4(5)	221.9(5)	220.2(7)
*RE*3–O3	1×	233.6(6)	231.0(9)	228.3(6)	226.2(5)	225.3(5)	225.0(7)
*RE*3–O5	1×	249.5(6)	248.8(8)	244.7(5)	243.3(5)	242.3(5)	239.7(7)
*RE*3–O2	1×	253.2(6)	250.7(8)	248.9(6)	249.0(5)	247.2(5)	244.7(7)
*RE*3–Br1	1×	316.0(1)	314.7(1)	313.9(4)	313.4(1)	312.5(1)	312.8(1)
*RE*3–Br2	1×	318.1(1)	316.7(2)	316.1(8)	315.6(1)	314.6(1)	314.6(1)
*RE*3–Br2′	1×	319.8(1)	319.1(1)	317.2(8)	316.1(1)	314.9(1)	314.9(1)
*RE*3–Br2″	1×	320.4(1)	319.1(2)	318.7(8)	318.3(1)	318.2(1)	317.6(1)
$[(As1)O_3]^{3-}$ anion							
As1–O1	1×	176.8(6)	178.3(8)	176.0(4)	175.3(5)	175.6(6)	176.0(7)
As1–O2	1×	178.4(6)	178.7(8)	178.6(6)	177.7(6)	179.0(5)	179.5(7)
As1–O3	1×	182.7(6)	184.2(8)	184.1(6)	184.8(5)	183.6(5)	183.8(8)
$[(As2)O_3]^{3-}$ anion							
As2–O4	1×	174.6(6)	174.4(8)	175.4(4)	174.4(5)	175.3(5)	176.0(6)
As2–O5	1×	181.2(5)	179.5(8)	181.8(5)	181.0(5)	181.1(5)	180.7(7)
As2–O6	1×	185.1(5)	184.6(8)	184.3(4)	185.1(5)	185.8(5)	184.2(6)

3.3. Crystal Structure of $RE_3Br_2[AsO_3][As_2O_5]$ (RE = Y and Dy–Yb)

The compounds with the composition $RE_3Br_2[AsO_3][As_2O_5]$ (*RE* = Y and Dy–Yb) crystallize isotypically to $RE_3Cl_2[AsO_3][As_2O_5]$ with *RE* = Sm–Gd [11,17] in the triclinic space group $P\bar{1}$ (no. 2) and lattice parameters from a = 539.15(4) pm, b = 870.68(6) pm, c = 1092.34(8), α = 90.661(2)°, β = 94.792(2)° and γ = 90.223(2)° for $Dy_3Br_2[AsO_3][As_2O_5]$ to a = 533.56(4) pm, b = 869.61(6) pm, c = 1076.70(8), α = 90.698(2)°, β = 94.785(2)° and γ = 90.053(2)° for $Yb_3Br_2[AsO_3][As_2O_5]$ with Z = 2. The crystal structure offers three different rare-earth metal(III) cation sites. $(RE1)^{3+}$ and $(RE2)^{3+}$ are both eight-fold coordinated exclusively by oxygen atoms, forming square $[(RE1,2)O_8]^{13-}$ prisms with d(Dy1–O) = 224–252 pm to d(Yb1–O) = 221–247 pm and d(Dy2–O) = 227–256 pm to d(Yb2–O) = 222–253 pm (Figure 7). These prisms join together via four common oxygen edges to form two-dimensional layers of composition $^{2}_{\infty}\{[(RE1/2)O^{e}_{8/2}]^{5-}\}$, which propagate parallel to the *ac*-plane (Figure 7). The third crystallographically diverse rare-earth metal (III) cation, on the other hand, shows both a different coordination environment and a different linkage pattern. In contrast to the cations $(RE1)^{3+}$ and $(RE2)^{3+}$, which carry solely oxygen atoms, contacts to the Br^- anions occur for the first time for $(RE3)^{3+}$, with four O^{2-} and four Br^- ligands erecting a square antiprism $[(RE3)O_4Br_4]^{9-}$ (Figure 7). Bond lengths from d(Dy3–O) = 222–248 pm and d(Dy3–Br) = 287–321 pm to d(Yb3–O) = 219–243 pm and d(Yb3–Br) = 285–322 pm have to be stated. The $(RE3)^{3+}$ cations are linked via common oxygen atoms to the previously described layers formed by the $[REO_8]^{13-}$ polyhedra centered by the $(RE1,2)^{3+}$ cations and graft above and below them (Figure 7). Amongst each other, the square $[(RE3)O_4Br_4]^{9-}$ antiprisms are linked via common edges of bromide anions, but only $(Br2)^-$ contributes to this linkage, whereas $(Br1)^-$ maintains only a single contact to this $(RE3)^{3+}$ cation. Thus, one-dimensional infinite double strands of the composition

$^{1}_{\infty}\{[(RE3)O^{t}_{4/1}(Br1)^{t}_{1/1}(Br2)^{e}_{3/3}]^{7-}\}$ are formed, which propagate along the *a*-axis (Figure 7). Bonds are formed between these two structural motifs along the *b*-axis via contacts between the double strands and the two-dimensional layers containing the $(RE1,2)^{3+}$ cations located above and below. Thus, two crystallographically different Br^{-} anions occur, which differ from each other by their different coordination spheres. While $(Br1)^{-}$ only has only one contact in the area effective for bonding to $(RE3)^{3+}$ cations with a bond length of around 286 pm, the $(Br2)^{-}$ anion is triple-coordinated and deflected by around 90 pm from the triangular plane formed by its three RE^{3+} ligands.

The crystal structure exhibits three different sites for the As^{3+} cations. The $(As1)^{3+}$ cation is only coordinated by three oxygen atoms and centers isolated ψ^{1}-tetrahedral $[AsO_3]^{3-}$ units, allowing a strong stereochemical lone-pair activity (Figure 8, *left*). A distinction must be made between different cases when analyzing the second coordination sphere. The oxygen atom O1 only forms bonds to two rare-earth metal(III) cations, while there are three for O2 and O3. This is the reason why the distance between the $(As1)^{3+}$ cation and O1 represents the shortest with *d*(As1–O1) = 174 pm for $Dy_3Br_2[AsO_3][As_2O_5]$ to *d*(As1–O1) = 175 pm for $Yb_3Br_2[AsO_3][As_2O_5]$, while the remaining bond lengths fall into the range of *d*(As1–O2/3) = 180–185 pm for $Dy_3Br_2[AsO_3][As_2O_5]$ to *d*(As1–O2/3) = 180–184 pm for $Yb_3Br_2[AsO_3][As_2O_5]$. The $(As2)^{3+}$ and $(As3)^{3+}$ cations are surrounded by a total of five oxygen atoms, forming a $[As_2O_5]^{4-}$ *pyro*-anion, in which one oxygen atom bridges both arsenic(III) cations according to $[O_2(As2)(O6)(As3)O_2]^{4-}$ (Figure 8, *right*), frequently addressed as "conversural ψ^{1}-bitetrahedron" [17]. The free electron pairs of both As^{3+} cations are oriented into the same direction. If the second coordination sphere of the As^{3+} cations is regarded, it becomes noticeable that the oxygen atoms O4 and O5 each form bonds to three RE^{3+} cations, while there are only two such contacts for O6 to O8. As a result, the lengths of the arsenic–oxygen bonds in the case of O4 and O5 with values of *d*(As2–O4/5) = 177–184 pm for $Dy_3Br_2[AsO_3][As_2O_5]$ to *d*(As2–O4/5) = 179–186 pm for $Yb_3Br_2[AsO_3][As_2O_5]$ are somewhat longer than those of O7 and O8, which range between *d*(As3–O7/8) = 174–177 pm for $Dy_3Br_2[AsO_3][As_2O_5]$ and *d*(As3–O7/8) = 175–176 pm for $Yb_3Br_2[AsO_3][As_2O_5]$. Of all those occurring in the entire crystal structure, the bridging oxygen atom O6 always shows the largest value in relation to any As^{3+} cations in terms of bond lengths (*d*(As2/3–O6) = 186–196 pm for $Dy_3Br_2[AsO_3][As_2O_5]$ to *d*(As2/3–O6) = 186–196 pm for $Yb_3Br_2[AsO_3][As_2O_5]$) with distances about 15 pm longer than those of the remaining arsenic–oxygen bonds. This fact gives the *pyro*-anion $[As_2O_5]^{4-}$ a highly asymmetric shape with ∢(As2–O6–As3) bond angles from 116° for *RE* = Dy to 115° for *RE* = Yb.

Within the crystal structure, channels are left behind between the bromide anion and rare-earth metal strands, into which the free electron pairs of the As^{3+} cations point (Figure 9).

Table 7 contains the crystallographic data for the $RE_3Br_2[AsO_3][As_2O_5]$ representatives with *RE* = Y and Dy–Yb, Table 8 summarizes the fractional atomic positions and U_{eq} values and Table 9 offers selected interatomic distances.

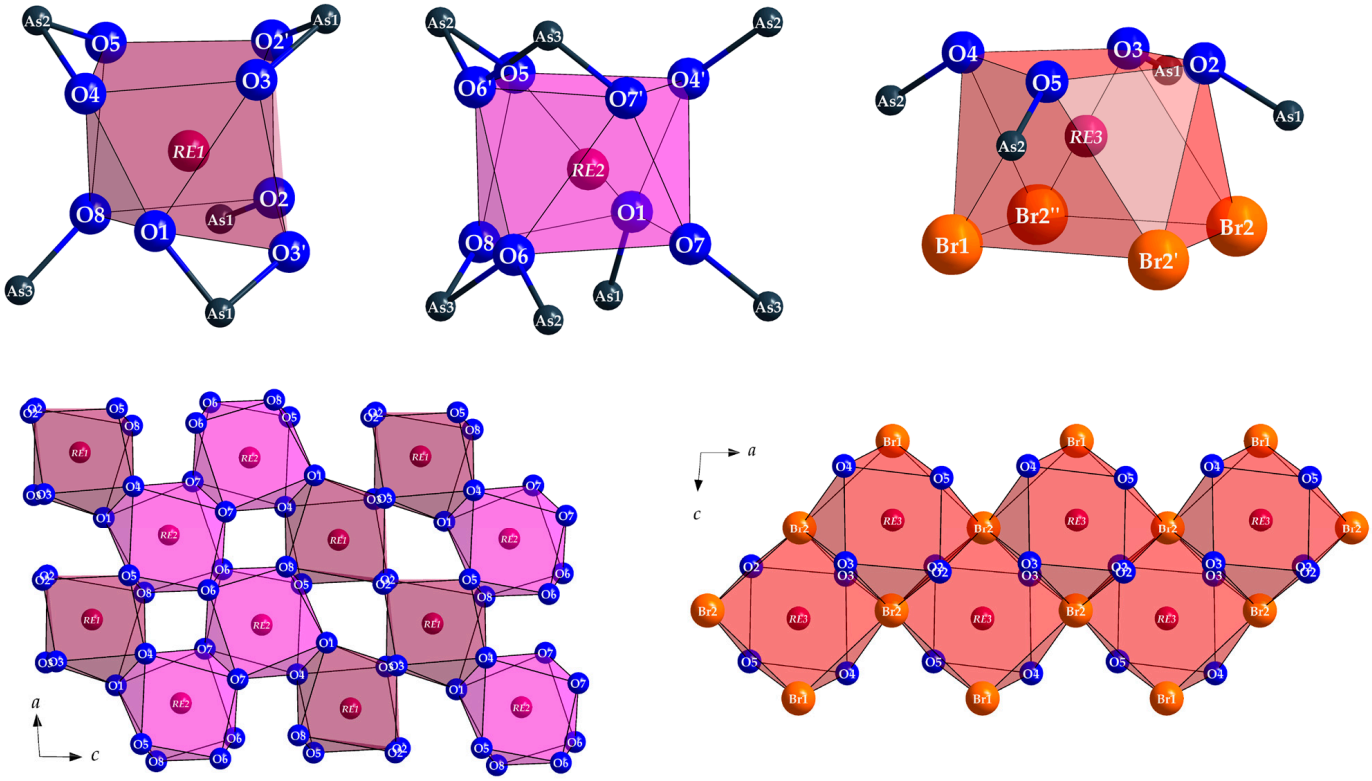

Figure 7. Distorted square antiprism $[(RE1)O_8]^{13-}$ (*top left*), highly distorted cube $[(RE2)O_8]^{13-}$ (*top mid*) and square antiprism $[(RE3)O_4Br_4]^{9-}$ (*top right*) with their environment of As^{3+} cations in the crystal structure of the $RE_3Br_2[AsO_3][As_2O_5]$ representatives (*RE* = Y and Dy–Yb) and their linkage to $^{2}_{\infty}\{[(RE1/2)O^{e}_{8/2}]^{5-}\}$ layers (*bottom left*) and $^{1}_{\infty}\{[(RE3)O_{4/1}^{t}(Br1)_{1/1}^{t}(Br2)_{3/3}^{e}]^{7-}\}$ double strands with singly coordinated $(Br1)^{-}$ and trigonally non-planar coordinated $(Br2)^{-}$ anions (*bottom right*).

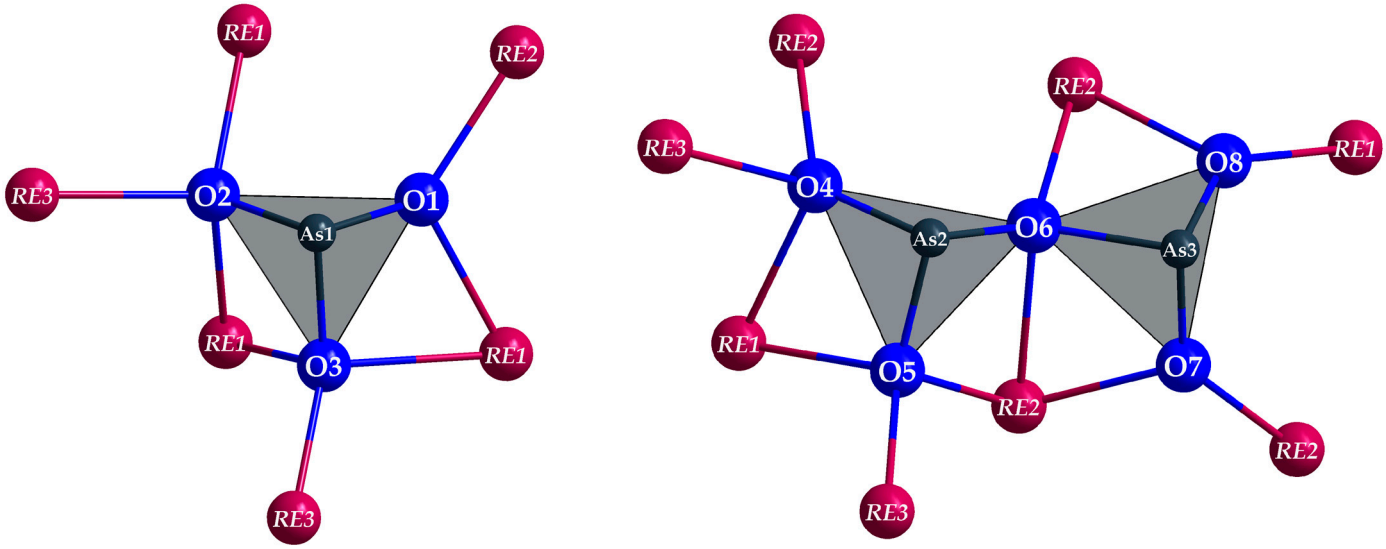

Figure 8. Irregular environment of RE^{3+} cations around the ψ^1-tetrahedral $[(As1)O_3]^{3-}$ anion and the conversural ψ^1-bitetrahedron $[(As2)(As3)O_5]^{4-}$ in the crystal structure of the $RE_3Br_2[AsO_3][As_2O_5]$ representatives with *RE* = Y and Dy–Yb.

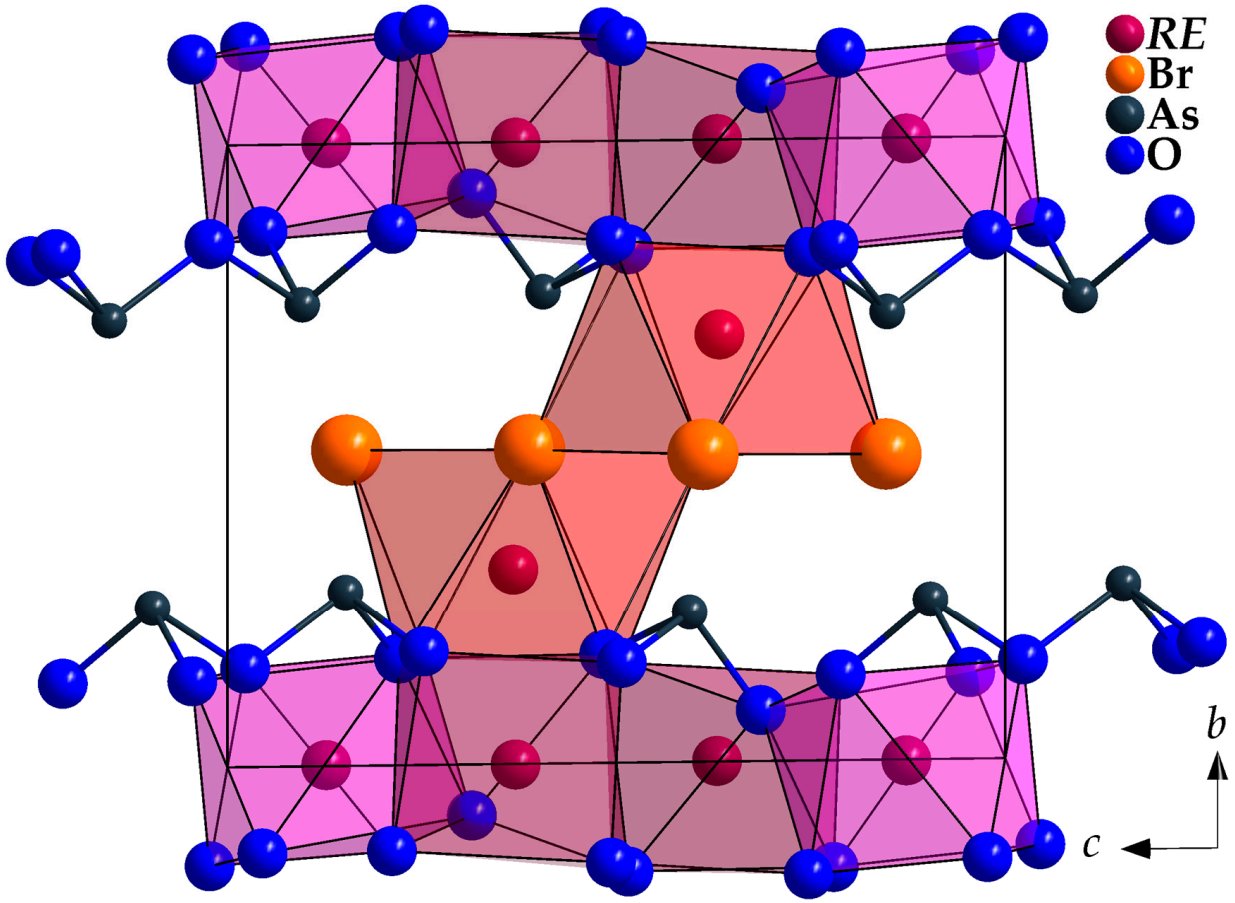

Figure 9. Extended unit cell of the $RE_3Br_2[AsO_3][As_2O_5]$ representatives with *RE* = Y and Dy–Yb.

Table 7. Crystallographic data of the $RE_3Br_2[AsO_3][As_2O_5]$ representatives with *RE* = Y and Dy–Yb and their determination.

$RE_3Br_2[AsO_3][As_2O_5]$		Y	Dy	Ho	Er	Tm	Yb
Crystal system				triclinic			
Space group				$P\bar{1}$			
Lattice parameters,	a/pm	538.06(4)	539.15(4)	537.54(4)	536.08(4)	534.76(4)	533.56(4)
	b/pm	870.48(6)	870.68(6)	870.39(6)	870.12(6)	869.81(6)	869.61(6)
	c/pm	1089.37(8)	1092.34(8)	1087.91(8)	1083.75(8)	1080.05(8)	1076.70(8)
	α/°	90.665(2)	90.661(2)	90.672(2)	90.683(2)	90.691(2)	90.698(2)
	β/°	94.790(2)	94.792(2)	94.798(2)	94.786(2)	94.784(2)	94.785(2)
	γ/°	90.189(2)	90.223(2)	90.173(2)	90.127(2)	90.088(2)	90.053(2)
Formula units, Z				2			
Calculated density, D_x/g·cm^{-3}		5.091	6.500	6.596	6.688	6.763	6.883
Molar volume, V_m/cm^3·mol^{-1}		153.07(7)	153.86(7)	152.72(7)	151.67(7)	150.73(7)	149.89(7)
Diffractometer				κ-CCD (Bruker-Nonius)			
Wavelength				Mo-K_α (λ = 71.07 pm)			
Electron sum, $F(000)$/e$^-$		700	862	868	874	880	886
Measurement limit, θ_{max}/°		27.48	33.05	27.48	27.48	27.48	27.48
Measurement range, $\pm h/\pm k/\pm l_{min/max}$		6/11/14	8/13/16	6/11/14	6/11/14	7/11/14	6/11/13
Observed reflections		16792	17816	18942	16738	21574	17988
Unique reflections		2331	3603	2323	2313	2286	2267
Absorption coefficient, μ/mm^{-1}		34.55	39.19	40.78	42.49	44.20	45.89
R_{int}/R_σ		0.093/0.040	0.085/0.048	0.075/0.037	0.074/0.037	0.066/0.026	0.083/0.034
R_1/R_1 with $\lvert F_o \rvert \geq 4\sigma(F_o)$		0.089/0.050	0.074/0.052	0.044/0.034	0.039/0.032	0.021/0.019	0.037/0.037
wR_2/Goof		0.098/1.021	0.133/1.033	0.083/1.046	0.071/1.083	0.043/1.109	0.092/1.081
Residual electron density, ρ/e$^-$·10^{-6}·pm^{-3}		−1.49/1.34	−3.15/3.24	−1.93/2.40	−2.07/2.16	−1.16/1.09	−2.36/2.43
CSD number		2330957	2330958	2330959	2330960	2330961	2330962

Table 8. Fractional atomic coordinates and coefficients of the equivalent isotropic displacement parameters for the $RE_3Br_2[AsO_3][As_2O_5]$ representatives with *RE* = Y and Dy–Yb.

Atom	*Wyckoff* Site	*x*/*a*	*y*/*b*	*z*/*c*	U_{eq}/pm^2
		$Y_3Br_2[AsO_3][As_2O_5]$			
Y1	2*i*	0.24645(19)	0.00069(13)	0.37073(11)	166(3)
Y2	2*i*	0.26430(19)	0.00226(13)	0.87296(11)	171(3)
Y3	2*i*	0.26578(19)	0.30990(13)	0.63195(11)	184(3)
Br1	2*i*	0.30265(19)	0.50700(13)	0.84590(11)	241(3)
Br2	2*i*	0.23049(19)	0.49526(13)	0.38910(11)	217(3)
As1	2*i*	0.27732(19)	0.75960(13)	0.59460(11)	172(3)
As2	2*i*	0.18944(19)	0.72135(13)	0.15158(11)	165(3)
As3	2*i*	0.18310(19)	0.25610(13)	0.09726(11)	173(3)
O1	2*i*	0.3677(13)	0.9207(9)	0.6873(7)	226(18)
O2	2*i*	0.0108(13)	0.8407(8)	0.5079(7)	186(17)
O3	2*i*	0.4994(13)	0.8262(8)	0.4858(7)	187(17)
O4	2*i*	0.4436(12)	0.8275(8)	0.2209(7)	179(17)
O5	2*i*	0.0197(12)	0.1823(8)	0.7481(7)	146(16)
O6	2*i*	0.0643(12)	0.8423(8)	0.0213(7)	168(17)
O7	2*i*	0.4142(13)	0.1363(9)	0.0443(7)	241(18)
O8	2*i*	0.0815(13)	0.1367(8)	0.2119(7)	188(17)
		$Dy_3Br_2[AsO_3][As_2O_5]$			
Dy1	2*i*	0.24538(11)	0.00096(7)	0.37052(6)	152(1)
Dy2	2*i*	0.26454(11)	0.00171(7)	0.87292(6)	153(1)
Dy3	2*i*	0.26669(11)	0.31302(7)	0.63249(6)	164(1)
Br1	2*i*	0.3030(3)	0.50816(18)	0.84651(14)	231(3)
Br2	2*i*	0.2309(3)	0.49457(17)	0.38864(13)	198(3)
As1	2*i*	0.2768(2)	0.75899(16)	0.59427(13)	158(3)
As2	2*i*	0.1889(2)	0.72071(16)	0.15190(13)	155(3)
As3	2*i*	0.1821(2)	0.25736(16)	0.09621(13)	155(3)
O1	2*i*	0.3660(18)	0.9183(12)	0.6857(9)	221(20)
O2	2*i*	0.0131(16)	0.8400(11)	0.5070(9)	147(17)
O3	2*i*	0.4965(17)	0.8255(11)	0.4844(9)	168(18)
O4	2*i*	0.4441(16)	0.8288(11)	0.2207(9)	158(17)
O5	2*i*	0.0200(18)	0.1822(12)	0.7475(9)	174(18)
O6	2*i*	0.0618(16)	0.8419(11)	0.0228(9)	158(17)
O7	2*i*	0.4109(18)	0.1386(11)	0.0451(9)	183(19)
O8	2*i*	0.0818(18)	0.1372(11)	0.2116(9)	177(18)
		$Ho_3Br_2[AsO_3][As_2O_5]$			
Ho1	2*i*	0.24644(7)	0.00085(5)	0.37100(4)	123(1)
Ho2	2*i*	0.26396(7)	0.00192(5)	0.87279(4)	123(1)
Ho3	2*i*	0.26531(7)	0.31149(5)	0.63203(4)	151(1)
Br1	2*i*	0.30222(17)	0.50643(12)	0.84633(9)	208(2)
Br2	2*i*	0.23100(16)	0.49506(11)	0.38905(8)	180(2)
As1	2*i*	0.27705(17)	0.75895(11)	0.59450(9)	143(2)
As2	2*i*	0.19021(17)	0.72145(11)	0.15191(9)	146(2)
As3	2*i*	0.18328(17)	0.25670(11)	0.09680(9)	145(2)
O1	2*i*	0.3681(11)	0.9203(8)	0.6874(6)	192(15)
O2	2*i*	0.0111(11)	0.8403(7)	0.5084(6)	108(12)
O3	2*i*	0.4991(11)	0.8283(8)	0.4859(6)	151(14)
O4	2*i*	0.4438(11)	0.8261(8)	0.2207(6)	163(14)
O5	2*i*	0.0207(11)	0.1810(8)	0.7479(6)	150(14)
O6	2*i*	0.0598(11)	0.8430(7)	0.0216(6)	152(14)
O7	2*i*	0.4133(11)	0.1378(7)	0.0432(6)	155(14)
O8	2*i*	0.0824(11)	0.1368(8)	0.2122(6)	165(14)
		$Er_3Br_2[AsO_3][As_2O_5]$			
Er1	2*i*	0.24639(7)	0.00057(5)	0.37118(4)	143(1)
Er2	2*i*	0.26408(7)	0.00229(5)	0.87282(4)	143(1)
Er3	2*i*	0.26480(7)	0.30989(5)	0.63183(4)	164(1)
Br1	2*i*	0.30195(18)	0.50585(12)	0.84580(9)	218(2)
Br2	2*i*	0.23051(17)	0.49557(11)	0.38950(9)	195(2)
As1	2*i*	0.27795(17)	0.75918(11)	0.59523(9)	151(2)
As2	2*i*	0.19065(17)	0.72116(11)	0.15179(9)	149(2)
As3	2*i*	0.18349(17)	0.25634(11)	0.09761(9)	151(2)
O1	2*i*	0.3713(12)	0.9190(8)	0.6891(6)	199(15)
O2	2*i*	0.0121(12)	0.8418(8)	0.5080(6)	152(14)
O3	2*i*	0.4982(12)	0.8284(8)	0.4859(6)	156(14)
O4	2*i*	0.4479(12)	0.8283(8)	0.2218(6)	174(14)
O5	2*i*	0.0193(12)	0.1804(8)	0.7474(6)	157(14)
O6	2*i*	0.0634(12)	0.8440(8)	0.0223(6)	164(14)
O7	2*i*	0.4136(12)	0.1373(8)	0.0444(6)	171(14)
O8	2*i*	0.0810(12)	0.1363(8)	0.2129(6)	168(14)

Table 8. *Cont.*

Atom	*Wyckoff* Site	*x*/*a*	*y*/*b*	*z*/*c*	U_{eq}/pm^2
		$Tm_3Br_2[AsO_3][As_2O_5]$			
Tm1	2*i*	0.24704(4)	0.00003(3)	0.37102(2)	93(1)
Tm2	2*i*	0.26454(4)	0.00269(3)	0.87266(2)	92(1)
Tm3	2*i*	0.26456(4)	0.30786(3)	0.63165(2)	108(1)
Br1	2*i*	0.30173(11)	0.50478(7)	0.84510(5)	163(1)
Br2	2*i*	0.23078(10)	0.49554(6)	0.38983(5)	147(1)
As1	2*i*	0.27809(10)	0.75946(6)	0.59570(5)	94(1)
As2	2*i*	0.19064(10)	0.72049(6)	0.15175(5)	90(1)
As3	2*i*	0.18288(10)	0.25530(6)	0.09807(5)	94(1)
O1	2*i*	0.3736(7)	0.9187(4)	0.6895(3)	140(8)
O2	2*i*	0.0108(7)	0.8427(4)	0.5087(3)	88(7)
O3	2*i*	0.4987(7)	0.8288(4)	0.4857(3)	94(7)
O4	2*i*	0.4485(7)	0.8276(4)	0.2222(3)	114(8)
O5	2*i*	0.0185(7)	0.1801(4)	0.7469(3)	96(7)
O6	2*i*	0.0630(7)	0.8439(4)	0.0220(3)	112(8)
O7	2*i*	0.4143(7)	0.1355(4)	0.0445(3)	108(8)
O8	2*i*	0.0795(7)	0.1355(4)	0.2134(3)	105(8)
		$Yb_3Br_2[AsO_3][As_2O_5]$			
Yb1	2*i*	0.24714(11)	−0.00059(7)	0.37125(5)	144(2)
Yb2	2*i*	0.26475(11)	0.00341(7)	0.87265(5)	144(2)
Yb3	2*i*	0.26418(11)	0.30675(7)	0.63146(5)	165(2)
Br1	2*i*	0.3011(2)	0.50392(18)	0.84506(13)	214(3)
Br2	2*i*	0.2309(2)	0.49578(17)	0.38989(12)	202(3)
As1	2*i*	0.2788(2)	0.75968(17)	0.59596(12)	153(3)
As2	2*i*	0.1910(2)	0.72064(17)	0.15149(12)	143(3)
As3	2*i*	0.1830(2)	0.25445(17)	0.09896(12)	151(3)
O1	2*i*	0.3755(17)	0.9179(12)	0.6902(9)	229(22)
O2	2*i*	0.0125(16)	0.8431(11)	0.5085(8)	129(17)
O3	2*i*	0.4981(17)	0.8298(11)	0.4856(8)	145(18)
O4	2*i*	0.4479(16)	0.8311(12)	0.2227(8)	160(19)
O5	2*i*	0.0196(16)	0.1772(11)	0.7462(8)	134(17)
O6	2*i*	0.0630(16)	0.8450(11)	0.0217(9)	159(19)
O7	2*i*	0.4147(17)	0.1337(11)	0.0445(8)	145(18)
O8	2*i*	0.0787(17)	0.1338(12)	0.2128(9)	173(19)

Table 9. Selected interatomic distances (d/pm) for the $RE_3Br_2[AsO_3][As_2O_5]$ representatives with RE = Y and Dy–Yb.

RE		Y	Dy	Ho	Er	Tm	Yb
$[(RE1)O_8]^{13-}$ polyhedron							
*RE*1–O8	1×	223.2(7)	223.5(9)	222.7(6)	221.8(6)	221.0(4)	220.9(9)
*RE*1–O1	1×	232.4(7)	234.0(10)	232.1(6)	231.2(7)	229.6(4)	228.9(10)
*RE*1–O3	1×	234.6(7)	234.3(10)	233.1(6)	232.1(6)	231.0(4)	229.3(9)
*RE*1–O2	1×	241.8(7)	243.6(9)	241.3(6)	240.5(6)	239.2(4)	239.4(9)
*RE*1–O5	1×	242.8(7)	242.5(10)	242.3(6)	240.8(7)	239.6(4)	237.3(9)
*RE*1–O2′	1×	247.7(7)	247.0(9)	247.9(6)	245.7(6)	245.7(4)	244.0(9)
*RE*1–O3′	1×	248.2(8)	250.8(10)	246.7(6)	246.4(7)	245.9(4)	245.3(10)
*RE*1–O4	1×	251.1(7)	251.5(9)	252.1(6)	250.5(7)	249.6(4)	246.6(9)
$[(RE2)O_8]^{13-}$ polyhedron							
*RE*2–O7	1×	224.5(7)	226.6(9)	225.8(6)	223.1(7)	223.0(4)	221.7(9)
*RE*2–O1	1×	224.9(8)	227.3(11)	224.6(6)	224.6(7)	222.4(4)	221.8(10)
*RE*2–O7′	1×	227.8(9)	229.6(10)	227.5(6)	227.5(7)	226.2(4)	224.7(9)
*RE*2–O8	1×	233.5(7)	233.9(9)	233.5(6)	232.8(7)	231.9(4)	230.5(10)
*RE*2–O5	1×	240.9(7)	241.9(10)	239.8(6)	239.4(6)	239.1(4)	236.7(9)
*RE*2–O4	1×	245.0(7)	244.5(9)	245.6(6)	242.9(6)	242.3(4)	240.2(9)
*RE*2–O6	1×	245.8(7)	248.0(9)	246.6(6)	245.3(7)	245.2(4)	244.4(9)
*RE*2–O6′	1×	257.0(7)	256.2(10)	254.6(6)	254.4(6)	253.9(4)	252.8(10)
$[(RE3)O_4Br_4]^{9-}$ polyhedron							
*RE*3–O5	1×	221.1(7)	222.3(9)	221.6(6)	220.8(6)	219.5(4)	219.1(9)
*RE*3–O3	1×	221.2(7)	222.8(9)	223.0(6)	222.0(6)	220.4(4)	220.0(9)
*RE*3–O2	1×	241.1(8)	243.4(10)	241.9(6)	241.0(7)	239.9(4)	239.3(9)
*RE*3–O4	1×	246.7(7)	248.4(10)	246.6(7)	244.5(7)	242.5(4)	243.1(9)
*RE*3–Br1	1×	287.1(2)	286.7(2)	286.0(1)	285.5(1)	284.9(6)	284.5(2)
*RE*3–Br2	1×	310.7(2)	310.6(2)	309.7(1)	309.2(1)	308.9(6)	308.7(2)
*RE*3–Br2′	1×	316.2(2)	316.2(2)	315.3(1)	314.6(1)	314.9(6)	314.6(2)
*RE*3–Br2″	1×	321.8(2)	320.6(2)	321.0(1)	321.4(1)	321.9(6)	321.9(2)
$[(As1)O_3]^{3-}$ anion							
As1–O1	1×	176.2(8)	174.2(11)	176.4(7)	176.0(7)	175.6(4)	175.1(11)
As1–O2	1×	180.1(7)	179.6(9)	179.4(6)	180.0(6)	180.2(4)	179.6(9)
As1–O3	1×	184.8(7)	185.2(9)	185.3(6)	184.6(6)	184.9(4)	184.4(9)
$[(As2)(As3)O_5]^{4-}$ anion							
As2–O4	1×	176.0(7)	177.3(9)	174.8(6)	177.5(7)	177.6(4)	178.7(9)
As2–O5	1×	183.1(7)	184.0(9)	184.0(6)	183.9(7)	183.8(4)	185.8(9)
As2–O6	1×	185.9(7)	185.8(9)	186.9(6)	185.9(6)	186.0(4)	186.2(9)
As3–O8	1×	175.4(7)	176.5(9)	176.1(6)	176.0(6)	175.7(4)	174.9(10)
As3–O7	1×	175.5(7)	173.6(10)	174.7(6)	174.2(7)	175.0(4)	175.6(9)
As3–O6	1×	196.3(7)	196.1(9)	195.0(6)	197.1(7)	195.9(4)	196.1(9)

3.4. Crystal-Structure Comparison

The rare-earth metal(III) bromide oxoarsenates(III) of formula type $RE_5Br_3[AsO_3]_4$ in the *A*- (*RE* = La and Ce) and *B*-type structure (*RE* = Pr, Nd and Sm–Tb) exhibit very similar structural motifs, if only all features are considered. The anionic environments of the RE^{3+} cations are almost identical, although the polyhedra of the $(RE2)^{3+}$ cations in the *A*-type resemble more of a square antiprism, while, in the *B*-type, they are more similar to a cube. The distances between the rare-earth metal and oxygen develop according to the lanthanoid contraction with no particular exceptions. The same applies to the anionic environment of the As^{3+} cations, as here are no real differences too. By stacking several layers, however, the differences become clear, as both structures represent stacking variants. In the *A*-type, there is a one-third offset from layer to layer, so that two particles of the following layers come to rest below a gap in one layer before the next gap occurs (Figure 10, *left*). As a result, every fourth bromide layer is congruent. The *B*-type does not show this behavior, because, here, the gaps of each layer lie directly on top of each other and are therefore congruent, creating additional channels along [100] (Figure 10, *right*). To summarize, it can be said that the *A*-type follows an ABC layer sequence, and the *B*-type is just an AAA variation.

At first glance, it is not noticeable that the compositions $RE_5Br_3[AsO_3]_4$ and $RE_3Br_2[AsO_3][As_2O_5]$ have a lot in common, but they share the completely same building blocks, except that, in the latter, there are two ψ^1-tetrahedral $[AsO_3]^{3-}$ anions, which are conversurally connected to $[As_2O_5]^{4-}$ units. If the bromide anions and oxygen atoms in both empirical formulae are brought to the same denominator, the following juxtaposition is obtained: $RE_5Br_3As_4O_{12}$ (for $RE_5Br_3[AsO_3]_4$) versus $RE_{4.5}Br_3As_{4.5}O_{12}$ (for $RE_3Br_2[AsO_3][As_2O_5]$). This shows that there has been a thinning of the rare-earth metal RE^{3+} and, at the same time, an enrichment of the arsenic As^{3+} in the sum formula by one-half each. This manifests structurally in a way that the $(RE3)^{3+}$ cations are thinned out and, instead of the double layers ${}^{2}_{\infty}\{[(RE3)O\,{}^{t}_{4/1}\,(Br1)\,{}^{v}_{1/2}\,(Br2)\,{}^{e}_{3/3}\,]^{6.5-}\}$, only double strands ${}^{1}_{\infty}\{[(RE3)O^{t}_{4/1}(Br1)^{t}_{1/1}(Br2)^{e}_{3/3}]^{7-}\}$ are able to be formed, and, on the other hand, instead of isolated $[AsO_3]^{3-}$ units, higher condensed oxoarsenates(III) with $[As_2O_5]^{4-}$ anions occur.

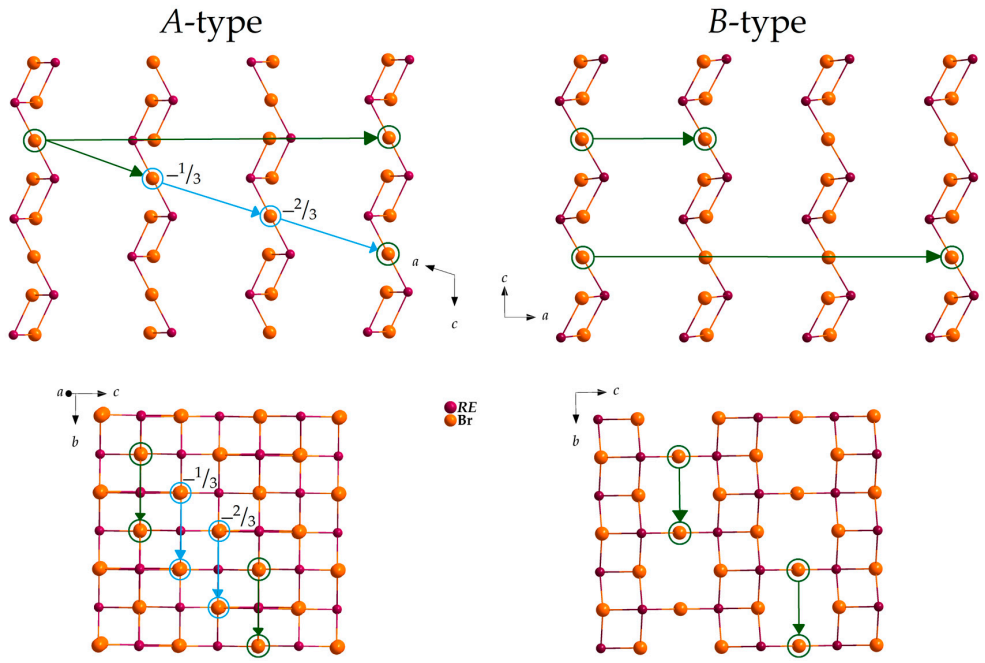

Figure 10. Comparison of the stacking sequence of the Br^- anions in the *A*-type (*left*) and *B*-type structure (*right*) of the $RE_5Br_3[AsO_3]_4$ representatives (*RE* = La–Nd and Sm–Tb) in side view (*top*) and top view (*bottom*) with highlighted positions of selected $(Br1)^-$ anions.

4. Conclusions

With a total of fourteen different representatives in three different structures, the range of rare-earth metal(III) bromide oxoarsenates(III) has been considerably expanded and supplemented. Future research must show whether the composition $RE_5Br_3[AsO_3]_4$ and $RE_3Br_2[AsO_3][As_2O_5]$ can also exist in parallel. Furthermore, the β angle in the *B*-type structure approaches closer and closer to 90°, which raises the question whether a structurally novel *C*-type for the heavier lanthanides might be formed, showing orthorhombic symmetry. Furthermore, under the synthetic conditions reported in this article, it was not possible to realize one of the two compositions for *RE* = Lu. Here, high-pressure experiments would be conceivable to realize an eightfold coordination for Lu^{3+}, as this tends to prefer six- or sevenfold coordination in contrast to other rare-earth metals.

Author Contributions: Conceptualization, R.J.C.L. and T.S.; methodology, R.J.C.L.; software, R.J.C.L.; validation, R.J.C.L.; formal analysis, R.J.C.L.; investigation, R.J.C.L., F.L., F.C.G. and F.C.Z.; resources, R.J.C.L.; data curation, R.J.C.L. and T.S.; writing—original draft preparation, R.J.C.L. and T.S.; writing—review and editing, R.J.C.L. and T.S.; visualization, R.J.C.L.; supervision, T.S.; project

administration, T.S.; funding acquisition, T.S. All authors have read and agreed to the published version of the manuscript.

Funding: This research received no external funding.

Data Availability Statement: Data are available from the authors upon request.

Acknowledgments: The authors thank Falk Lissner for the single-crystal X-ray diffraction measurements.

Conflicts of Interest: The authors declare that the research was conducted in the absence of any commercial or financial relationships that could be construed as a potential conflict of interest.

References

1. Schmidt, M.; Oppermann, H.; Henning, C.; Henn, R.W.; Gmelin, E.; Söger, N. Untersuchungen zu Bismutseltenerdoxidhalogeniden der Zusammensetzung Bi_2SEO_4X (*X* = Cl, Br, I). *Z. Anorg. Allg. Chem.* **2000**, *626*, 125–135. [CrossRef]
2. Locke, R.J.C.; Goerigk, F.C.; Paterlini, V.; Mudring, A.-V.; Schleid, T. Light from three different lanthanum oxoantimonate(III) bromides: (La,Sb)OBr, $La_5Br_3[SbO_3]_4$ and $LaSb_2O_4Br$. *Z. Anorg. Allg. Chem.* **2025**. *submitted*.
3. Goerigk, F.C.; Schleid, T. Composition and crystal structure of $SmSb_2O_4Cl$ revisited and the analogy of $Sm_{1.5}Sb_{1.5}O_4Br$. *Z. Anorg. Allg. Chem.* **2019**, *645*, 1079–1084. [CrossRef]
4. Locke, R.J.C.; Goerigk, F.C.; Schäfer, M.J.; Höppe, H.A.; Schleid, T. Synthesis, crystal structures and spectroscopic properties of pure YSb_2O_4Br and YSb_2O_4Cl as well as Eu^{3+}- and Tb^{3+}-doped samples. *Roy. Soc. Chem. Adv.* **2022**, *12*, 640–647. [CrossRef] [PubMed]
5. Locke, R.J.C.; Weis, M.; Schleid, T. $LnSb_2O_4Br$ (*Ln* = Nd and Er) and $Sb_4O_5Br_2$. Lanthanoid-bearing and -free antimony(III) oxide bromides. *Z. Anorg. Allg. Chem.* **2024**, *650*, e202300243. [CrossRef]
6. Goerigk, F.C.; Paterlini, V.; Dorn, K.V.; Mudring, A.-V.; Schleid, T. Synthesis and Crystal Structure of the Short $LnSb_2O_4Br$ Series (*Ln* = Eu – Tb) and Luminescence Properties of Eu^{3+}-Doped Samples. *Crystals* **2020**, *10*, 1089. [CrossRef]
7. Locke, R.J.C.; Goerigk, F.C.; Schleid, T. Unconnected Bromide Layers in the Crystal Structure of $DySb_2O_4Br$. *Z. Kristallogr.* **2021**, *S41*, 78–79.
8. Locke, R.J.C.; Schleid, T. $TmSb_2O_4Br$: The first tetragonal lanthanoid oxoantimonate bromide without mixed-cation occupation. *Acta Crystallogr.* **2023**, *A79*, C777. [CrossRef]
9. Locke, R.J.C.; Bozenhardt, K.-N.; Goerigk, F.C.; Schleid, T. Three New Lanthanum Oxoantimonate(III) Halides: Synthesis and Crystal Structure of $La_5Cl_3[SbO_3]_4$, $La_2Sb_{12}O_{19}Br_4$ and $La_2Sb_{12}O_{19}I_4$. *Crystals* **2023**, *13*, 731. [CrossRef]
10. Ben Yahia, H.; Rodewald, U.C.; Pöttgen, R. Crystal Structure of $La_3OBr[AsO_3]_2$. *Z. Naturforsch.* **2010**, *65b*, 1289–1292. [CrossRef]
11. Goerigk, F.C.; Schander, S.; Wickleder, M.S.; Schleid, T. The Triclinic Lanthanoid(III) Halide Oxidoarsenates(III) $Sm_3Cl_2[As_2O_5][AsO_3]$ and $Tm_3Br_2[As_2O_5][AsO_3]$. *Z. Anorg. Allg. Chem.* **2020**, *646*, 985–991. [CrossRef]
12. Herrendorf, W.; Bärnighausen, H. *HABITUS: Program for the Optimization of the Crystal Shape for Numerical Absorption Correction in X-SHAPE*; Version 1.06; Stoe & Cie: Darmstadt, Germany, 1999.
13. Sheldrick, G.M. *SHELXS-97 and SHELXL-97: Programs for Solution and Refinement of Crystal Structures from X-Ray Diffraction Data*; University of Göttingen: Göttingen, Germany, 1997.
14. Sheldrick, G.M. A short history of *SHELX*. *Acta Crystallogr.* **2008**, *A64*, 112–122. [CrossRef] [PubMed]
15. Kang, D.-H.; Schleid, T. $Ce_5Cl_3[AsO_3]_4$: The Second Chloride Oxoarsenate(III) of the Lanthanides, but the First One with Proper Crystallography. *Z. Kristallogr.* **2007**, *S25*, 98.
16. Goerigk, F.C.; Schander, S.; Ben Hamida, M.; Kang, D.-H.; Ledderboge, F.; Wickleder, M.S.; Schleid, T. Die monoklinen Seltenerdmetall(III)-Chlorid-Oxidoarsenate(III) mit der Zusammensetzung $SE_5Cl_3[AsO_3]_4$ (*SE* = La–Nd, Sm). *Z. Naturforsch.* **2019**, *74b*, 497–506. [CrossRef]
17. Schander, S.; Locke, R.J.C.; Wickleder, M.S.; Schleid, T. Two further members of the triclinic lanthanoid(III) chloride oxoarsenate(III) series $Ln_3Cl_2[AsO_3][As_2O_5]$ with *Ln* = Eu and Gd. *Z. Naturforsch.* **2024**, *79b*, 529–533. [CrossRef]